



Munc13 activates the Munc18-1/syntaxin-1 complex and enables Munc18-1 to prime SNARE assembly

Xianping Wang^{1,†}, Jihong Gong^{1,†}, Le Zhu^{1,†}, Shen Wang¹ , Xiaoyu Yang¹, Yuanyuan Xu¹, Xiaofei Yang² & Cong Ma^{1,3,*} 

Abstract

Priming of synaptic vesicles involves Munc13-catalyzed transition of the Munc18-1/syntaxin-1 complex to the SNARE complex in the presence of SNAP-25 and synaptobrevin-2; Munc13 drives opening of syntaxin-1 via the MUN domain while Munc18-1 primes SNARE assembly via domain 3a. However, the underlying mechanism remains unclear. In this study, we have identified a number of residues in domain 3a of Munc18-1 that are crucial for Munc13 and Munc18-1 actions in SNARE complex assembly and synaptic vesicle priming. Our results showed that two residues (Q301/K308) at the side of domain 3a mediate the interaction between the Munc18-1/syntaxin-1 complex and the MUN domain. This interaction enables the MUN domain to drive the opening of syntaxin-1 linker region, thereby leading to the extension of domain 3a and promoting synaptobrevin-2 binding. In addition, we identified two residues (K332/K333) at the bottom of domain 3a that mediate the interaction between Munc18-1 and the SNARE motif of syntaxin-1. This interaction ensures Munc18-1 to persistently associate with syntaxin-1 during the conformational change of syntaxin-1 from closed to open, which reinforces the role of Munc18-1 in templating SNARE assembly. Taken together, our data suggest a mechanism by which Munc13 activates the Munc18-1/syntaxin-1 complex and enables Munc18-1 to prime SNARE assembly.

Keywords Munc13; Munc18-1; SNARE complex assembly; synaptic exocytosis

Subject Category Membranes & Trafficking

DOI 10.15252/embj.2019103631 | Received 3 October 2019 | Revised 20 May 2020 | Accepted 2 June 2020 | Published online 9 July 2020

The EMBO Journal (2020) 39: e103631

Introduction

Neurotransmitter release by exocytosis involves the docking of synaptic vesicles at presynaptic active zones, the priming of the vesicles to assume a “ready-for-fusion” state, and the fast fusion of the vesicles with the plasma membrane in response to Ca²⁺ (Südhof

& Rizo, 2011; Jahn & Fasshauer, 2012). Central to this process are the SNARE proteins, including syntaxin-1 (Syx1) and SNAP-25 (SN25) on the plasma membrane as well as synaptobrevin-2 (Syb2) on the vesicles (Brunger, 2005; Jahn & Scheller, 2006). The SNAREs form a four-helical bundle called the SNARE complex to bring the two membranes into close proximity and to drive membrane fusion (Sutton *et al*, 1998; Weber *et al*, 1998; Stein *et al*, 2009). To achieve the exquisite regulation of exocytosis, a number of SNARE regulatory proteins are required, including the SM (Sec1/Munc18-like) protein Munc18-1 and the CATCHR (complexes associated with tethering containing helical rods)-related protein Munc13 (Malsam *et al*, 2008; Jahn & Fasshauer, 2012; Rizo & Südhof, 2012; Rizo & Xu, 2015).

Munc18-1 orchestrates SNARE complex assembly via multiple interactions with the SNAREs (Südhof & Rothman, 2009; Collins & Martin, 2015; Rizo & Xu, 2015). Munc18-1 binds tightly to Syx1 to form a Munc18-1/Syx1 heterodimeric complex (Misura *et al*, 2000; Burkhardt *et al*, 2008; Colbert *et al*, 2013) to chaperone Syx1 for proper targeting to the plasma membrane (Arunachalam *et al*, 2008; Han *et al*, 2009). In this complex, Munc18-1 locks Syx1 in a “closed” conformation, rendering it unable to assemble with SN25 and Syb2 (Dulubova *et al*, 1999; Yang *et al*, 2000). This binding mode accords with vesicle docking (Voets *et al*, 2001; Toonen *et al*, 2006; Han *et al*, 2011) as it allows vesicle accumulation around the plasma membrane without leading to fusion. At the stage of vesicle priming, Munc18-1 loosens its clamping of Syx1 while simultaneously binding Syb2 to initiate SNARE assembly (Parisotto *et al*, 2014; Baker *et al*, 2015; Sitariska *et al*, 2017; Jiao *et al*, 2018; Wang *et al*, 2019). At the fusion stage, Munc18-1 interacts with the assembled or assembling SNARE complex to promote membrane fusion (Dulubova *et al*, 2007; Shen *et al*, 2007; Rodkey *et al*, 2008; Tareste *et al*, 2008; Ma *et al*, 2015).

In addition to Munc18-1, synaptic exocytosis requires Munc13 (Rizo & Südhof, 2012; Brunger *et al*, 2019). Munc13-1 is abundant at the presynaptic terminal and plays an essential role in vesicle priming (Augustin *et al*, 1999; Varoqueaux *et al*, 2002; Imig *et al*, 2014). Increasing evidence has shown that Munc13-1 catalyzes the transition from the Munc18-1/Syx1 complex to the SNARE complex in the presence of SN25 and Syb2 (Ma *et al*, 2011; Yang *et al*, 2015;

1 Key Laboratory of Molecular Biophysics of the Ministry of Education, College of Life Science and Technology, Huazhong University of Science and Technology, Wuhan, China

2 Key Laboratory of Cognitive Science, Hubei Key Laboratory of Medical Information Analysis and Tumor Diagnosis & Treatment, Laboratory of Membrane Ion Channels and Medicine, College of Biomedical Engineering, South-Central University for Nationalities, Wuhan, China

3 Institute of Brain Research, Huazhong University of Science and Technology, Wuhan, China

*Corresponding author. Tel: +86 13317196805; E-mail: cong.ma@hust.edu.cn

†These authors contributed equally to this work

Lai *et al*, 2017; Wang *et al*, 2017; Kreutzberger *et al*, 2019). The transition involves at least two conformational changes within the Munc18-1/Syx1 complex, including (i) in the linker region of Syx1, which changes its conformation from a defined structure to a random coil to initiate the opening of Syx1 (Misura *et al*, 2000; Margittai *et al*, 2003; Wang *et al*, 2017); and (ii) in domain 3a of Munc18-1, which switches its conformation from a “bent” structure to an “extended” conformation to serve as a template essential for Syb2 binding and SNARE association (Hu *et al*, 2011; Han *et al*, 2014; Parisotto *et al*, 2014; Munch *et al*, 2016; Sitarska *et al*, 2017; Jiao *et al*, 2018). In line with this notion, both a Munc18-1 P335A mutation that promotes domain 3a extension and a Syx1 L165A/E166A (“LEAA”) mutation that helps to facilitate opening of the Syx1 linker region were observed to enhance exocytosis in neurons and neuroendocrine cells (Dulubova *et al*, 1999; Gerber *et al*, 2008; Martin *et al*, 2013; Han *et al*, 2014; Munch *et al*, 2016; Park *et al*, 2017). Moreover, either P335A or LEAA was found to partially rescue a defect in exocytosis in *unc-13* null *Caenorhabditis elegans* (Richmond *et al*, 2001; Hammarlund *et al*, 2007; Park *et al*, 2017), suggesting a strong correlation between Munc13 action and the two conformational changes within the Munc18-1/Syx1 complex.

In this study, we have identified a number of residues in the Munc18-1 domain 3a that are important for Munc13-catalyzed transition from the Munc18-1/Syx1 complex to the SNARE complex. Mutating these residues exerts no effect on Syx1 transport to the plasma membrane but severely impairs vesicle priming and fusion in mammalian neurons. Our data showed that the Munc13-1 MUN domain binds the Munc18-1/Syx1 complex and drives the opening of the Syx1 linker region via an interaction with the side face of domain 3a. The open of the Syx1 linker region leads to the extension of domain 3a, thereby promoting binding of Syb2 to the Munc18-1/Syx1 complex. In addition, our data identified an interaction between the bottom of domain 3a and the SNARE motif of Syx1. This binding enables Munc18-1 to associate with the SNARE motif of Syx1 during the transit of Syx1 from the Munc18-1/Syx1 complex to the SNARE complex, which is crucial for templating SNARE assembly by Munc18-1.

Results

Mutational analysis of the Munc18-1 domain 3a

Previous studies have shown that the Munc13-1 MUN domain catalyzes the transition from the Munc18-1/Syx1 complex to the SNARE

complex. In addition, increasing evidence suggests the functional importance of the Munc18-1 domain 3a in SNARE complex assembly. Hence, we aimed to explore the potential functional interplay between domain 3a and the MUN domain in the transition from the Munc18-1/Syx1 complex to the SNARE complex.

As revealed by the crystal structure of the Munc18-1/Syx1 complex (Fig 1A), two antiparallel helices (H11 and H12) connected by a hinge loop constitute the exterior part of the bent structure of domain 3a. We rationally designed a series of mutations on the solvent-accessible surfaces of helices H11, H12, and the hinge loop (Fig 1A), including mutations that had been described in previous studies, for example, the D326K, K332E/K333E, P335A, and L348R mutations (Han *et al*, 2013; Parisotto *et al*, 2014; Sitarska *et al*, 2017). All the mutants, except for P335A, exhibited similar elution volumes to that of wild-type (WT) Munc18-1, as assessed by gel filtration (Fig 1B and Table EV1). It is noteworthy that the lower elution volume observed for the P335A mutant is likely due to the self-association (dimerization) of Munc18-1. However, all the mutants bound to monomeric Syx1 (the cytoplasmic domain of Syx1, residues 2–253) and yielded a heterodimeric complex similar to that of WT Munc18-1, as judged by gel filtration (Fig 1B and Table EV2), which was indicative of their effectiveness in binding the closed Syx1.

We next explored the potential defects caused by these mutations in MUN-catalyzed transition from the Munc18-1/Syx1 complex to the SNARE complex. By using a previously established native-PAGE assay (Yang *et al*, 2015; Wang *et al*, 2019), we indeed observed that Syx1 bound to the Munc18-1 mutant P335A or D326K allowed the transition to occur even in the absence of the MUN domain, albeit with various extents (Fig 1C and D), consistent to previous results (Park *et al*, 2017; Sitarska *et al*, 2017). The observed “gain-of-function” effects arise likely because either P335A or D326K contributes to extend the conformation of domain 3a, as previously suggested. Conversely, a number of mutations were found to remarkably inhibit MUN-catalyzed transition to the SNARE complex, including Q301A and K308A in helix H11, K332E/K333E (KKEE) in the hinge loop, and L348R in helix H12 (Fig 1C and D). Note that there is a little trace of SNARE complex formation in the background of the native PAGE, which is likely due to a little amount of free Syx1 that escapes from Munc18-1 clamping in our Munc18-1/Syx1 samples.

Next, we re-examined the Q301A/K308A (QKAA), KKEE, and L348R mutants using both FRET and lipid-mixing assays as previously established (Yang *et al*, 2015). Consistently, the FRET experiments showed that the three mutations abrogated MUN-catalyzed

Figure 1. Residues in the Munc18-1 domain 3a essential for MUN-catalyzed transition from the Munc18-1/Syx1 complex to the SNARE complex.

- A Structure overview of the Munc18-1/Syx1 complex (pdb entry: 3C98). Mutating residues are highlighted in red below the domain depiction and shown as yellow sticks in the structure.
- B Elution volumes (peak positions) of the Munc18-1 mutants in the absence (top) and presence (bottom) of Syx1 using size-exclusion chromatography on Superdex-200 column.
- C Effects of the domain 3a mutations on MUN-catalyzed transition detected by native-PAGE assay. Components addition was indicated on the top of every lane.
- D Quantitative analysis of the integrated densities of Munc18-1/Syx1 bands in C.
- E Effects of the QKAA, KKEE, and L348R mutations on MUN-catalyzed transition detected by FRET assay. Schematic diagram is shown on the top of the chart. FRET between BODIPY FL-labeled Syb2 (donor) and TMR-labeled SN25 (acceptor) was monitored.
- F Effects of the QKAA, KKEE, and L348R mutations on lipid mixing between liposomes with Munc18-1/Syx1 and liposomes containing Syb2 in the presence of Munc13 (M13), SN25, and Syt1/Ca²⁺. Illustration of the reactions is shown on the top of the chart.

Data information: Representative gels and/or traces displayed are from one of three independent replicates. In D–F, all bar charts are presented as mean values ± SD, *n* = 3 technical replicates.

Source data are available online for this figure.

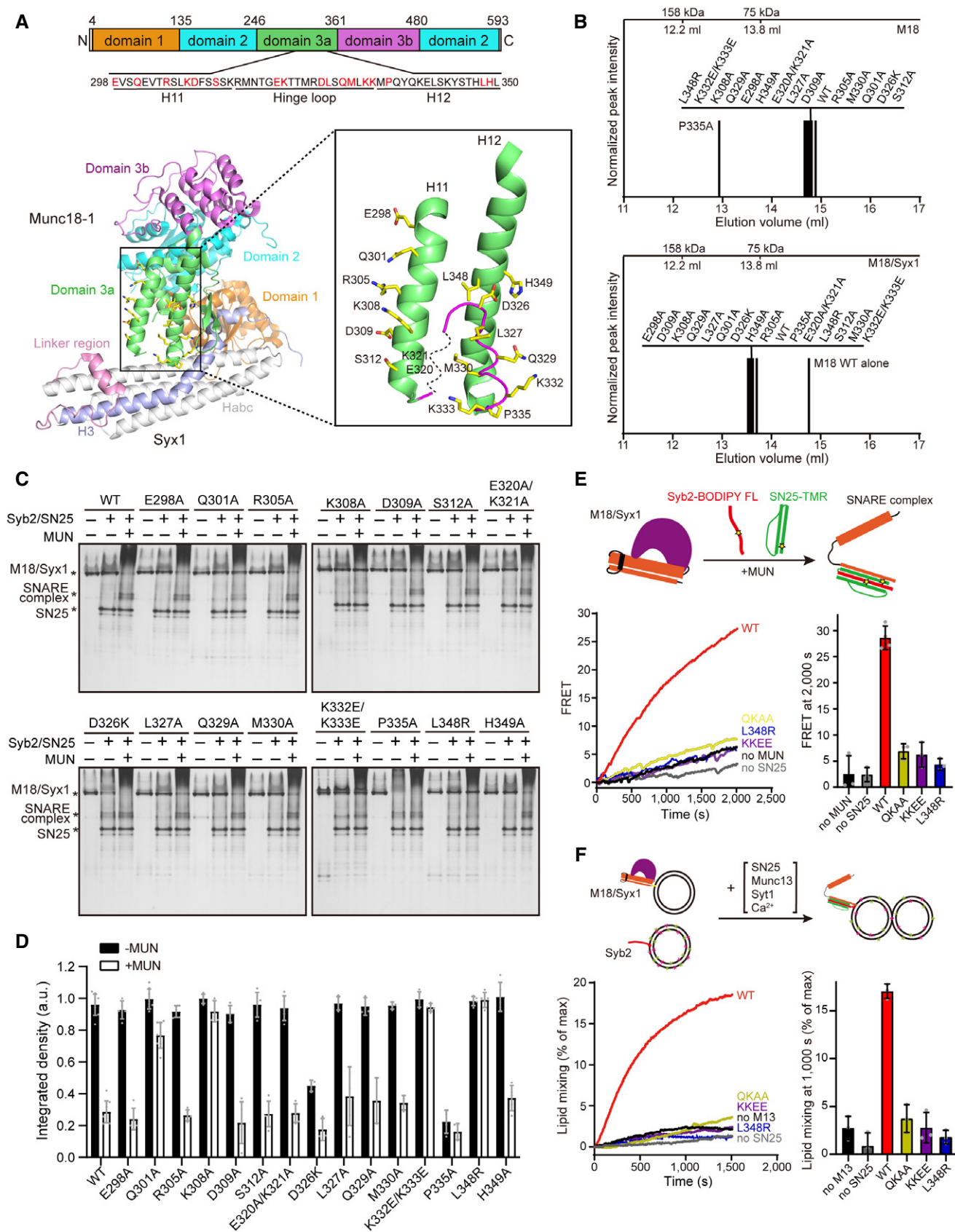


Figure 1.

transition to the SNARE complex (Fig 1E). Likewise, the mutations failed to promote lipid mixing between liposomes containing the Munc18-1/Syx1 complex and liposomes bearing Syb2 with the addition of SN25, synaptotagmin-1 (Syt1), and Munc13-1 (C₁-C₂B-MUN) in the presence of Ca²⁺ (Fig 1F). Additional experiments demonstrated that the single mutation (Q301A or K308A) could abrogate lipid mixing (Appendix Fig S1). Note that the C₁-C₂B-MUN fragment exhibited higher activity than the isolated MUN domain in liposome fusion, owing to its specific membrane binding mediated by the C₁ and C₂B domains (Ma *et al.*, 2013). Furthermore, sequence alignment showed that these functionally important residues are highly conserved among Munc18-1 homologues in various species (Appendix Fig S2). Together, upon extensive screening using combined *in vitro* approaches, we have identified a number of residues in domain 3a of Munc18-1 that are essential for MUN-catalyzed SNARE complex assembly and membrane fusion.

Functional analysis of domain 3a in synaptic vesicle exocytosis

To substantiate our *in vitro* results, we tested for functional defects of the mutations identified above in synaptic vesicle (SV) exocytosis by using a knockdown (KD)-rescue approach in cultured mouse cortex neurons. The endogenous Munc18-1 expression level was suppressed by virally delivered shRNAs (Fig EV1A). Expression of Munc18-1 WT rescued the spontaneous mini-inhibitory postsynaptic current (mIPSC) frequency and action potential-evoked inhibitory postsynaptic current (evoked IPSC) amplitude and charge transfer (Fig 2A and B). However, the expression of the QKAA, KKEE, and L348R mutants failed to rescue the mIPSC and evoked IPSC (Fig 2A and B). The mIPSC amplitude was unaffected in all conditions, excluding the major postsynaptic effect caused by the Munc18-1 KD (Fig 2A). Note that overexpression of the three mutants in WT background neurons reduced the mIPSC (Appendix Fig S3), confirming their dominant-negative effect. In addition, these mutants impaired mini-excitatory postsynaptic current (mEPSC) frequency (Appendix Fig S4). All the mutants were steadily expressed in cultured neurons (Fig EV1A) and targeted to synapses (Fig EV1B), and supported synaptic formation without influencing the number and size of synapses (Fig EV1B–D).

The abrogation of exocytosis could be due to defective priming. A classic assay to analyze vesicle priming involves the application of hypertonic sucrose to induce exocytosis in a Ca²⁺-independent manner (Rosenmund & Stevens, 1996). Using this assay, we characterized the size of the readily releasable pool (RRP) of vesicles with application of sucrose solution. The significant reduction in the RRP

observed in neurons deficient in Munc18-1 was rescued by expressing WT Munc18-1 (Fig 2C). However, the QKAA, KKEE, and L348R mutants were unable to rescue the reduction in the RRP (Fig 2C), implying their impairment to support vesicle priming.

Compared to the “loss-of-function” mutants, we found that the P335A mutant successfully rescued both mIPSC and evoked IPSC as well as RRP (Fig 2A–C), in a manner similar to WT Munc18-1. Additional experiments showed that even a single mutation (Q301A or K308A) produced a severe reduction in the mIPSC, evoked IPSC and RRP (Fig EV2) and that the defect caused by the L348R mutation in SV exocytosis is consistent with previous results showing that the same mutation impairs secretion in chromaffin cells (Munch *et al.*, 2016). Unexpectedly, the KKEE mutant, which was previously found to support dense-core vesicle (DCV) secretion in PC12 cells (Han *et al.*, 2013), caused an impairment of SV exocytosis in cultured neurons (Fig 2), indicating that SV exocytosis is more sensitive to this mutation than DCV exocytosis. In addition, the KKEE mutation combined with an additional 5-residue insertion (KKEE + MPQKK) produced a strong defect in SV exocytosis in cultured neurons (Fig EV2), similar to that observed for DCV secretion in PC12 cells (Han *et al.*, 2013). The raw data for the above electrophysiological experiments are included in Appendix Fig S5. The data obtained in cultured neurons are highly consistent with our *in vitro* data, reinforcing the critical roles of the residues Q301/K308, L348, and K332/K333 in priming of SV.

Activity of domain 3a in Syx1 transport

The impaired interaction between Munc18-1 and the closed Syx1 would lead to retention of either one in the cytosol thus influencing vesicle docking and priming. To test this, we determined whether these mutants affected Syx1 transport to the cell surface using a HEK293T cell system. The membrane probe DiD was applied as an indicator to track the plasma membrane compartment (Servant *et al.*, 1999). The majority of EGFP-Munc18-1 or mCherry2-Syx1 was sequestered in the cytosol when each was expressed separately (Fig 3A), while coexpression enhanced the colocalization of both proteins at the cell surface (Fig 3B–D). The QKAA, KKEE, and L348R mutants all supported Syx1 transport to the cell surface (Fig 3B–D), similar to WT Munc18-1.

Next, we carried out a GST pull-down experiment to directly measure the binding of the mutants with Syx1. Similar to WT Munc18-1, the three mutants interacted with Syx1 (Fig 3E). The binding data are consistent with the gel filtration results (Fig 1B) showing that these mutants can form a heterodimeric complex with

Figure 2. The Munc18-1 domain 3a is essential for synaptic vesicle exocytosis.

- A Representative traces (left), summary graphs of normalized frequency (middle), and normalized amplitude (right) of mIPSCs recorded from cultured cortical neurons that were infected with lentivirus expressing Munc18-1 WT or mutants, with or without Munc18-1 shRNAs (Control, *n* = 25; None, *n* = 17; WT, *n* = 17; QKAA, *n* = 18; KKEE, *n* = 16; P335A, *n* = 23; L348R, *n* = 21).
- B Sample traces (left), summary graphs of normalized amplitude (middle), and normalized charge transfer (right) of evoked IPSCs recorded from neurons as described in panel A (Control, *n* = 19; None, *n* = 19; WT, *n* = 19; QKAA, *n* = 13; KKEE, *n* = 18; P335A, *n* = 17; L348R, *n* = 21).
- C Sample traces (left) and quantification of the normalized charge transfer evoked by hypertonic sucrose (right) recorded from the neurons described in panel A (Control, *n* = 17; None, *n* = 13; WT, *n* = 17; QKAA, *n* = 17; KKEE, *n* = 18; P335A, *n* = 15; L348R, *n* = 14).

Data information: In A–C, data are shown as mean values ± SEM; **P* < 0.05; ***P* < 0.01; ****P* < 0.001. Statistical significance was analyzed by Student's *t*-test. A number of neurons analyzed are from three independent cultures, and data from different cultures are normalized. The raw data are shown in Appendix Fig S3.

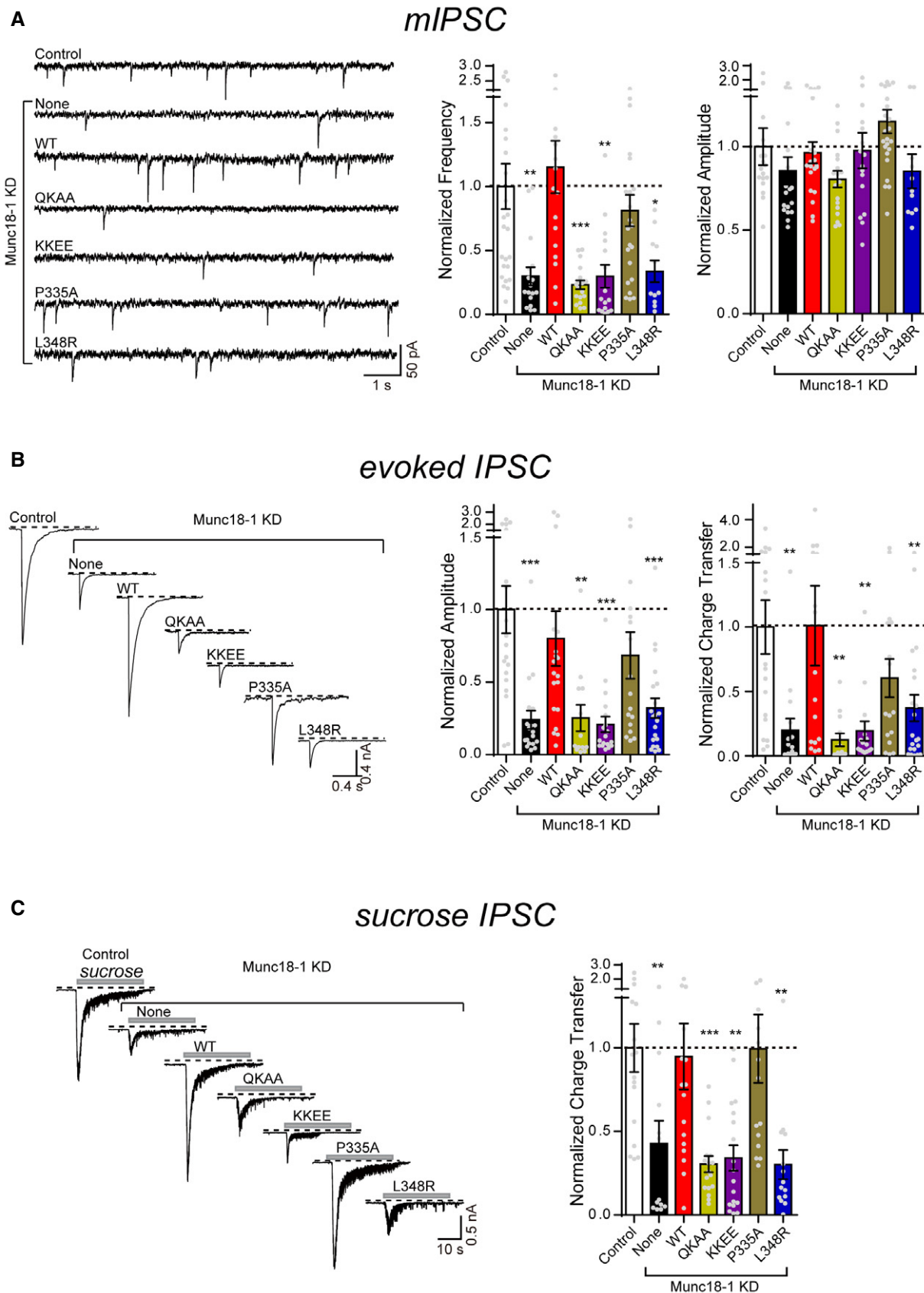


Figure 2.

Syx1. Taken together, these results rule out the possibility that the QKAA, KKEE, and L348R mutants abrogate vesicle priming via affecting Syx1 transport.

Domain 3a is involved in MUN-catalyzed opening of the Syx1 linker region

Previous work has revealed that the MUN domain of Munc13-1 binds the Munc18-1/Syx1 complex to catalyze opening of the Syx1 linker region even in the absence of SN25 and Syb2 (Wang *et al*, 2017). We explored whether the above mutations in domain 3a influence MUN activity in opening the Syx1 linker region in the absence of SN25 and Syb2 by using established single-molecule FRET (smFRET) assay (Joo & Ha, 2012; Wang *et al*, 2017). Considering that Syx1 (2–253) contains only one cysteine at residue 145, we designed a double FRET-labeled version of Syx1 (residues 2–253, C145S/S95C/S171C) to monitor the conformational change of the Syx1 linker region (Fig 4A, Wang *et al*, 2017). S95C and S171C were labeled stochastically with Alexa-555 and Alexa-647, respectively, via maleimide covalent linkage and immobilized on a passivated surface via His-tag/PEG-NTA-Co²⁺ (Fig 4A).

Consistent with previous results, dual-labeled Syx1 exhibited high FRET efficiency when bound to Munc18-1 (black curve) and showed low FRET efficiency when assembled into the SNARE complex (cyan curve) (Fig 4B), corresponding to the expected closed and open conformations of the Syx1 linker region, respectively. Notably, in the absence of SN25 and Syb2, the addition of the MUN domain to the Munc18-1/Syx1 complex led to the formation of a population of Syx1 with intermediate FRET efficiency (red curve in Fig 4B), confirming the ability of the MUN domain to open the Syx1 linker region within the Munc18-1/Syx1 complex. Similarly, Syx1 bound to the three individual mutants (QKAA, KKEE, or L348R) resulted in a high FRET efficiency in the absence of the MUN domain (Fig 4C–F, blue curves), indicating the tightly closed conformation of the Syx1 linker region in these complexes. Intriguingly, with the addition of the MUN domain to Syx1 bound to the QKAA, KKEE, or L348R mutants in the absence of SN25 and Syb2, only the QKAA mutant failed to result in the shifting of FRET distribution of Syx1 from high to intermediate FRET efficiency (Fig 4C–F, purple curves), suggesting that only the QKAA mutant impairs MUN activity in opening the Syx1 linker region.

Based on the above results, it is expected that Q301/K308 on helix H11 of domain 3a may be involved in the interaction between

the Munc18-1/Syx1 complex and the MUN domain. To test this point, we directly compared the effects of the mutations using GST pull-down experiments combined with immunoblotting. Indeed, the WT, KKEE, and L348R mutants supported the interaction, but the QKAA mutant and other single mutant (Q301A or K308A) failed to support the interaction (Figs 4G and EV3), suggesting that Q301/K308 in domain 3a is required for the interaction between the MUN domain and the Munc18-1/Syx1 complex.

Next, we investigated whether QKAA altered the intrinsic properties of Munc18-1 in SNARE complex assembly using the Munc18-1/Syx1^{LEAA} complex as the starting complex. As the LEAA mutation can destabilize the Syx1 linker region, the transition from the Munc18-1/Syx1^{LEAA} complex to the SNARE complex can be achieved in the presence of SN25 and Syb2 without the MUN domain. In this system (Munc13-independent SNARE assembly system, Appendix Fig S6), we observed when starting with the Munc18-1^{WT}/Syx1^{LEAA} complex, addition of SN25 and Syb2 led to SNARE complex assembly (red curve). Similar SNARE assembly rate and content were observed when starting with the Munc18-1^{QKAA}/Syx1^{LEAA} complex (blue curve). These data suggest that the QKAA mutation seems unlikely to impair Munc18-1 activity in SNARE assembly, as both Munc18-1 WT and the QKAA mutant behaved similarly in Munc13-independent SNARE assembly. As a control, neither the Munc18-1^{WT}/Syx1^{WT} complex nor the Munc18-1^{QKAA}/Syx1^{WT} complex was able to transit to the SNARE complex even with the addition of SN25 and Syb2 (black and purple curves, respectively), because Munc13 was lacking and the Syx1 linker region still adopts a closed conformation. These results suggest that the QKAA mutation does not influence the intrinsic activity of Munc18-1 in SNARE assembly.

The MUN domain enables the extension of domain 3a

The transition from the Munc18-1/Syx1 complex to the SNARE complex involves both the opening of the Syx1 linker region and the extension of domain 3a. Unfortunately, direct measurement of conformational change of domain 3a by smFRET is impractical due to the existence of a large number of cysteine residues in Munc18-1, which renders specific FRET-pair labeling difficult. Alternatively, we characterized the “bent-to-extended” conformational change of domain 3a by measuring the binding of Syb2 to the Munc18-1/Syx1 complex in the absence and presence of the MUN domain (Fig 5A), considering that the extended rather than the bent structure of domain 3a is compatible with

Figure 3. Monitoring Syx1 transport in HEK293T cell.

- A Representative images of HEK293T cells transfected with mCherry2-Syx1 or EGFP-Munc18-1. Lipophilic dye DiD (1,1-dioctadecyl-3,3,3-tetramethylindodicarbocyanine) was used as the plasma membrane marker.
- B Representative images of HEK293T cells co-transfected with mCherry2-Syx1 and EGFP-labeled WT or mutants of Munc18-1.
- C, D Summary graphs of the membrane distribution of Syx1 (C) and Munc18-1 WT or mutants (D) quantified by the ratio of fluorescence at the plasma membrane (PM) to the total fluorescence in the whole cell (total). DiD is the PM marker. Numbers of pictures analyzed are shown as follows: no Syx1, $n = 14$; no M18, $n = 15$; WT, $n = 24$; QKAA, $n = 23$; KKEE, $n = 12$; L348R, $n = 22$.
- E Munc18-1 mutants retain interaction with Syx1 shown by GST pull-down experiment. A representative gel displayed is from one of three independent replicates.

Data information: In C and D, a number of pictures analyzed are from three independent experiments; one picture contains one to three intact cells. Data shown in summary graphs are mean values \pm SEM. Statistical significance was analyzed by Student's *t*-test. *** $P < 0.001$; **** $P < 0.0001$. Scale bar: 20 μ m. The scale bar applies to all images in each panel.

Source data are available online for this figure.

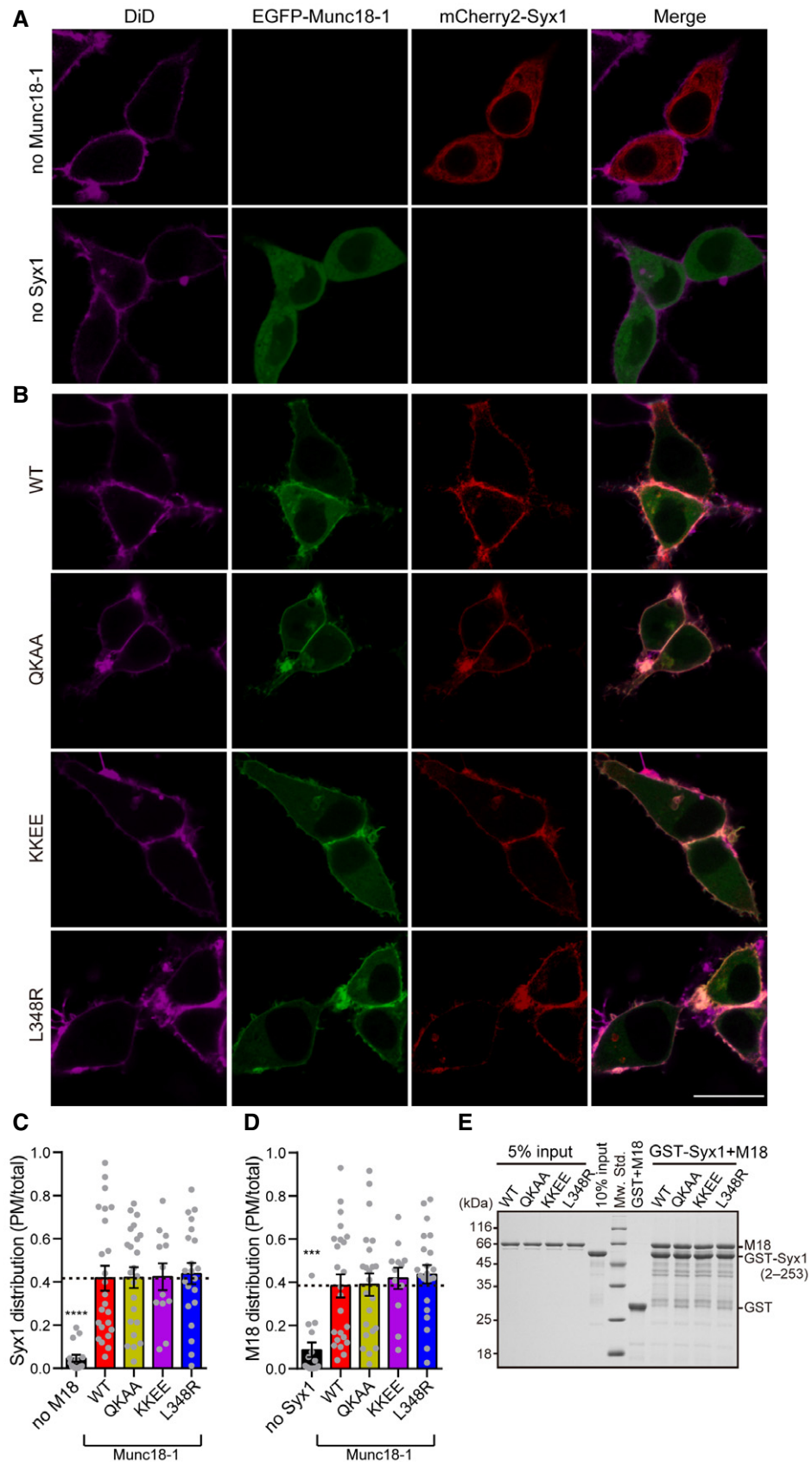


Figure 3.

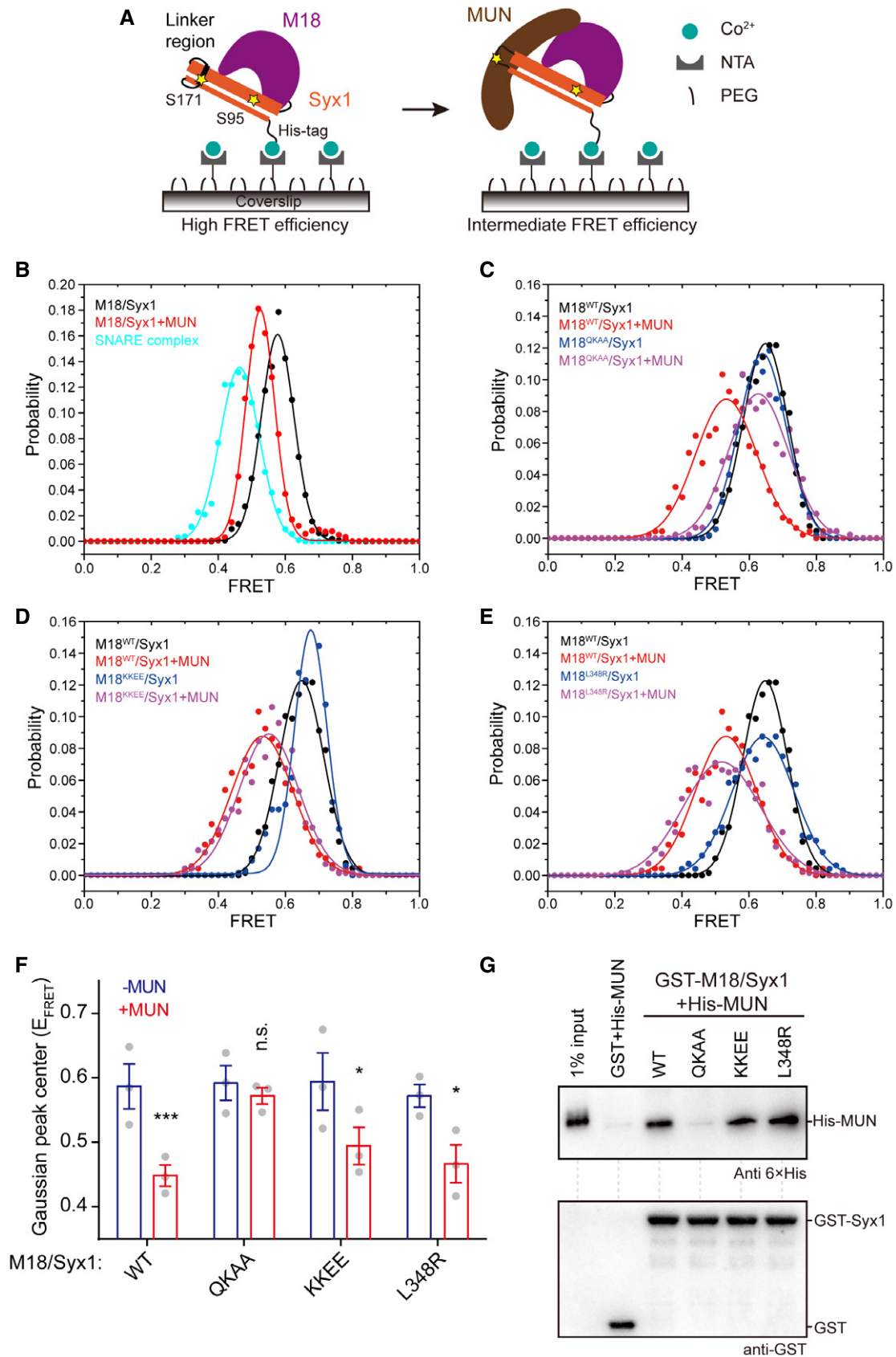


Figure 4.

Figure 4. Munc13 catalyzes opening of the Syx1 linker region via binding to the Munc18-1 domain 3a.

- A Schematic depiction of smFRET assay. Positions of FRET label pair (S95C/S171C) in Syx1 are indicated as yellow pentagrams. 6 × His-tagged Syx1 bound to Munc18-1 was immobilized on coverslip coated with PEG/PEG-NTA-Co²⁺. Syx1 linker region is colored by black.
- B Example histograms of smFRET efficiency of Syx1 in complex with Munc18-1 WT in the absence and presence of the MUN domain, and within the SNARE complex.
- C–E Example histograms of smFRET efficiency of Syx1 bound to Munc18-1 QKAA (C), KKEE (D), and L348R (E) in the absence or presence of the MUN domain. The QKAA mutation strongly impaired the shift of smFRET efficiency in the presence of the MUN domain.
- F Quantitative results of the Gaussian peak center positions of the FRET efficiency distributions in C–E.
- G Effects of QKAA, KKEE, and L348R mutations on the interaction between the Munc18-1/Syx1 complex and the MUN domain by GST pull-down assay combined with immunoblotting. Results were shown with 6 × His-tag antibody and GST-tag antibody.

Data information: In F, data are presented as mean values ± SEM, n.s., not significant; **P* < 0.05; ****P* < 0.001, *n* = 3 technical replicates. Statistical significance was analyzed by Student's *t*-test. In G, a representative gel displayed is from one of three independent replicates. Source data are available online for this figure.

Syb2 binding (Parisotto *et al*, 2014; Baker *et al*, 2015; Sitarska *et al*, 2017). Under our experimental conditions, GST-Syb2 did not bind isolated Munc18-1 (Appendix Fig S7). Similarly, no detectable binding was observed between GST-Syb2 and the Munc18-1/Syx1 complex (Fig 5B and C). Intriguingly, the presence of the MUN domain promoted binding of Syb2 to the Munc18-1/Syx1 complex (Fig 5B and C), suggesting that the MUN domain achieves the extension of domain 3a. Among the mutants, the P335A mutant supported the interaction between the Munc18-1/Syx1 complex and GST-Syb2 in the presence of the MUN domain (Appendix Fig S8). The KKEE mutant also supported the interaction, but the QKAA and L348R mutants failed (Fig 5B and C).

The binding defect caused by the L348R mutant was expected, as L348 is contained in the Syb2-binding groove in domain 3a based on the Vps33/Nyv1 structure and biochemical data (Parisotto *et al*, 2014; Baker *et al*, 2015; Sitarska *et al*, 2017). Compared to L348, the Q301 and K308 residues are distant from the Syb2-binding groove (Fig EV4). Hence, the binding defect caused by the QKAA mutant may arise from the abrogation of domain 3a extension. In conclusion, the QKAA mutation impairs MUN activity in opening the Syx1 linker region, thereby impairing domain 3a extension.

Potential coupling and consequences of the two conformational changes

The Munc18-1 P335A and Syx1 LEAA mutations were found to promote the extension of domain 3a and the opening of the Syx1 linker region, respectively (Parisotto *et al*, 2014; Wang *et al*, 2017); we next used the two mutants to investigate the potential coupling and consequences of the two conformational changes during the transition from the Munc18-1/Syx1 complex to the SNARE complex. Based on the ensemble FRET assay described in Fig 1E, we observed that the Syx1 LEAA mutation facilitated the transition in the presence of SN25 and Syb2 even when the MUN domain was absent (Fig 6A and B). No obvious enhancement was observed with further addition of the MUN domain (Fig 6A and B), suggesting that the Syx1 LEAA mutant almost completely bypasses the need for the MUN domain in the transition, leading to both the open of the Syx1 linker region and the extension of domain 3a. By comparison, although the Munc18-1 P335A mutation also accelerated the transition in the presence of SN25 and Syb2 when the MUN domain was absent (Fig 6A and B), this acceleration was moderate and could be further enhanced by the MUN domain (Fig 6A and B) to a level approximate to that resulting from the Syx1 LEAA mutation. These

data suggest that Munc18-1 P335A only results in the extension of domain 3a but does not lead to the open of the Syx1 linker region. Consistent with these results, smFRET experiments showed that the Syx1 linker region adopts a closed structure in Syx1 when bound to P335A, and it went through a conformational change (closed to open) upon the addition of the MUN domain (Fig 6C and D). These results, together with those in Figs 4 and 5, suggest that (i) the opening of the Syx1 linker region driven by the MUN domain represents an early event independent of the extension of domain 3a; and (ii) the opening of the Syx1 linker region leads to the extension of domain 3a, but not *vice versa*.

Conformational flexibility of domain 3a

To date, no structural information has been reported for isolated Munc18-1, as Munc18-1 alone is prone to aggregate at high concentrations (above 40 μM) unless it is bound to Syx1. We observed that the KKEE mutation, compared to the other mutations, dramatically enhanced the solubility (up to 200 μM) of Munc18-1 even in the absence of Syx1, which allowed us to solve the crystal structure of isolated Munc18-1 (KKEE). As the KKEE mutant behaves similar to WT Munc18-1 (Figs 3–5), this mutant provides an opportunity to characterize the structural features of isolated Munc18-1. The crystal structure was determined and refined to 3.4 Å in resolution (Table 1). The crystal contains two molecules per asymmetric unit, with one molecule packed against the other via domain 3a (Fig 7A). Compared to the bent structure of domain 3a observed in the WT Munc18-1/Syx1 complex, domain 3a adopts an extended conformation in isolated Munc18-1 (KKEE) (Fig 7B), similar to that observed in the structure of squid Sec1, Munc18-2, or Munc18-1 carrying the Syx4 N-peptide (Fig 7C). Superposition of these crystal structures showed that they share the same secondary structure, yet domain 1 and domain 3a in the Munc18 proteins are positioned at different angles, reflecting the rotational motion of both domains (Fig 7D). The intrinsic conformational flexibility of Munc18-1 is compatible with the distinct conformations of Syx1 (multiple Munc18-1/Syx1 intermediates). This finding suggests that the bent conformation of domain 3a is suited for binding to the closed Syx1 while the extending of domain 3a is more favorable once Munc18-1 no longer binds the closed Syx1. In our crystallization trials, the intrinsic flexibility of domain 3a allowed the preferential stabilization (dimerization) of the extended structure of domain 3a promoted by crystal packing. Hence, the structure is consistent with our notion that domain 3a is capable of extending its conformation during the opening of the Syx1 linker region.

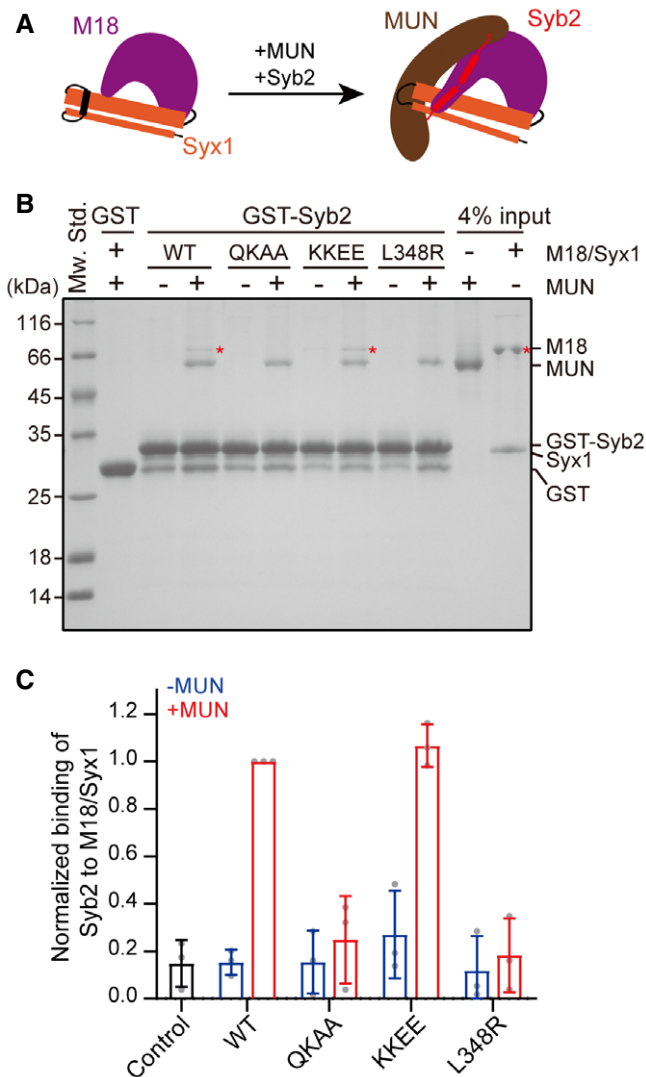


Figure 5. Munc13 promotes Syb2 binding to the Munc18-1/Syx1 complex.

A Schematic depiction of Syb2 binding to Munc18-1/Syx1 complex in the presence of MUN domain. The extended instead of bent conformation of domain 3a within the Munc18-1/Syx1 complex is compatible with Syb2 binding.

B Effects of the QKAA, KKEE, and L348R mutations on binding of Syb2 to Munc18-1/Syx1 complex in the presence and absence of MUN domain detected by GST pull-down assay. Bands of Munc18-1 are indicated with red asterisks.

C Quantification of the normalized binding of Syb2 to Munc18-1/Syx1 complex. Integrated intensities of Munc18-1 bands were quantified. QKAA and L348R, but not KKEE, disrupted Syb2 binding to the Munc18-1/Syx1 complex.

Data information: In B, a representative gel displayed is from one of three independent replicates. In C, data are presented as mean values \pm SD, $n = 3$ technical replicates.

Source data are available online for this figure.

Domain 3a binds the open form of Syx1

According to the Vps33/Nyv1 and Vps33/Vam3 binding modes (Baker et al, 2015), the templating role of domain 3a in SNARE

assembly would be associated with the interaction with the SNARE motif of Syb2 and Syx1. With the opening of Syx1 and the extension of domain 3a in the presence of the MUN domain, binding of the SNARE motif of Syb2 to domain 3a is achieved (Fig 5); however, whether domain 3a interacts with the open Syx1 (the SNARE motif of Syx1, termed Syx1-H3) remains unexplored. The K332 and K333 residues are positioned at the bottom face of domain 3a adjacent to Syx1-H3 (Fig 1A), implying the potential role of K332/K333 in mediating the H3 interaction. Measurement of actual binding between Munc18-1 and the H3 monomer was hindered by the assembly of the H3 tetramer *in vitro* (Misura et al, 2001). To solve this problem, we reconstituted a ternary complex comprising Munc18-1 together with Habc (residues 1–180) and H3 (residues 191–253) molecules (Fig 8A). As expected, Syx1-H3 failed to bind isolated Munc18-1 or Habc, as detected by gel filtration (Fig EV5). Strikingly, Syx1-H3 interacted simultaneously with Munc18-1 and Habc yielding a ternary complex (Fig 8B) with an elution volume similar to that of the Munc18-1/Syx1 (2–253) complex (Fig 8C), indicating the globally closed structure of Habc and H3 within the Munc18-1/H3/Habc complex (Fig 8A). Despite the architectural similarity, H3 in the Munc18-1/H3/Habc complex can transit into the SNARE complex upon the addition of SN25 and Syb2 in the absence of the MUN domain (Appendix Fig S9), reflecting an open form of H3 in the ternary complex. It is expected that this conformation of H3 resembles that of the Munc18-1/Syx1 complex containing the Syx1 LEAA mutation.

We then explored whether domain 3a mutations influence the assembly of H3 into the ternary complex. Similar to WT Munc18-1, the QKAA and L348R mutants maintained interactions with both Habc and H3, yielding a ternary complex (Fig 8D). However, the KKEE mutant impeded the formation of the ternary complex, as inferred from the remarkable lagging of the retention volume compared to that of WT Munc18-1 (Fig 8D). Note that the QKAA, L348R, and KKEE mutants all supported the Habc interaction in the absence of H3, similar to WT Munc18-1 (Fig 8E and F), suggesting that the KKEE mutant specifically hindered the assembly of H3 into the tertiary complex. Hence, these data identified an interaction between domain 3a and Syx1-H3. Taken together, these results suggest that K332/K333 constitutes a key site in domain 3a that mediates binding to the open Syx1 (Fig 8G). This binding enables Munc18-1 to persistently associate with Syx1 during the conformational change of Syx1 from closed to open.

Finally, we also tested whether the three mutations affect the interaction of Munc18-1 with the fully assembled SNARE complex. We observed that the QKAA, L348R, and KKEE mutants all bound the assembled SNARE complex as effectively as WT Munc18-1 using GST pull-down experiments (Appendix Fig S10), confirming that these mutations affect SNARE assembly in its early stage.

Discussion

Growing evidence indicates that Munc18 and Munc13 together assemble SNARE complexes and hereby enable synaptic vesicle exocytosis (Ma et al, 2011; Yang et al, 2015; Lai et al, 2017; Wang et al, 2017; Kreutzberger et al, 2019). In this process, the MUN domain of Munc13 catalyzes the transition from the Munc18-1/Syx1 complex to the SNARE complex in the presence of Syb2 and SN25 (Ma et al, 2011; Yang et al, 2015), but the

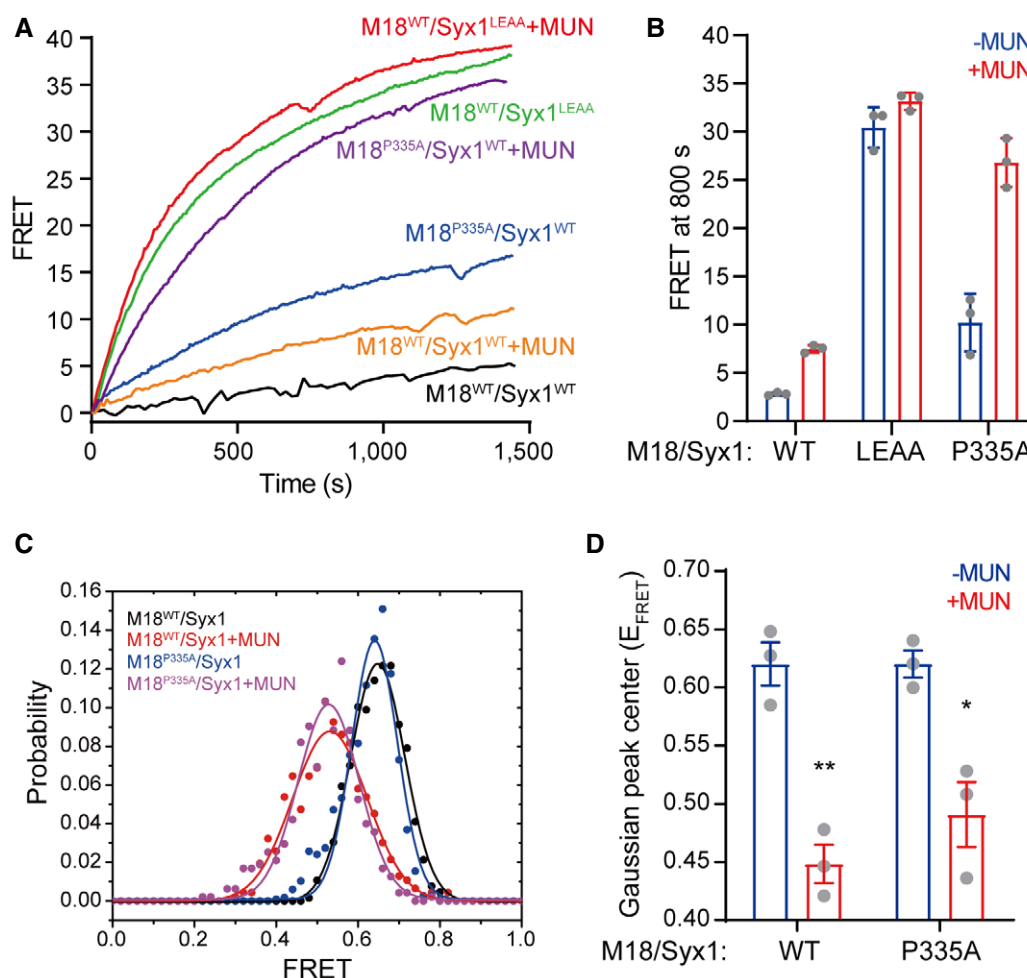


Figure 6. Potential interplay between the two conformational changes of Munc18-1 domain 3a and Syx1 linker region.

A Ensemble FRET assay showing the different effects of the Munc18-1 P335A mutation and the Syx1 LEAA mutation in the transition from the Munc18-1/Syx1 complex to the SNARE complex with and without the MUN domain. FRET signal between BODIPY FL-labeled Syb2 (donor) and TMR-labeled SN25 (acceptor) was monitored.

B Quantification of the FRET results in A.

C Single-molecule FRET assay showing the MUN domain drives the open of the Syx1 linker region independent of the conformational change of domain 3a. Example histograms of smFRET efficiency of Syx1 bound to Munc18-1 P335A mutant in the absence and presence of the MUN domain.

D Quantitative results of the Gaussian peak center positions of the FRET efficiency distributions in C.

Data information: In B, data are presented as mean values \pm SD, $n = 3$ technical replicates. In D, data are presented as mean values \pm SEM, $*P < 0.05$; $**P < 0.01$, $n = 3$ technical replicates. Statistical significance was analyzed by Student's t -test.

underlying molecular mechanism remains elusive. In this study, by the combined use of biophysical and biochemical approaches both *in vivo* and *in vitro*, we have revealed the mechanism by which Munc13 activates the Munc18-1/Syx1 complex and enables domain 3a to prime SNARE assembly.

In this study, we identified that two conserved residues (Q301 and K308, located in helix H11 of the Munc18-1 domain 3a) are essential for Munc13-dependent SNARE complex assembly and physiologically important for vesicle priming (Figs 1 and 2). Q301 and K308 mediate the interaction between the MUN domain and the Munc18-1/Syx1 complex; this interaction is required for MUN activity in catalyzing the opening of the Syx1 linker region (Fig 4). It is noteworthy that we cannot fully exclude the possibility that Q301 and K308 may also contribute to the activity of domain 3a in Syb2

binding, although the structural superposition of Munc18-1 and Vps33/Nyv1 shows that the two residues are positioned at a distance from the Syb2-binding groove (Fig EV4). Given that domain 3a and the Syx1 linker region are spatially adjacent to each other within the Munc18-1/Syx1 complex (Fig 1A), it is conceivable that multiple sites alongside domain 3a and the Syx1 linker region cooperate to form an ideal surface for MUN binding (Fig 9), rendering the MUN catalytic pocket (NF pocket, Yang *et al*, 2015) more accessible to its binding target in the Munc18-1/Syx1 complex. In line with this notion, previous studies found that the Syx1 linker region also participates in MUN binding to the Munc18-1/Syx1 complex and MUN activity in catalyzing the opening of the Syx1 linker region (Yang *et al*, 2015; Wang *et al*, 2017). This cooperative binding mode is in agreement with previous observations that the

Table 1. Data collection and refinement statistics.

Crystal	Munc18-1 ^{KKEE}
Data collection	
Space group	P4 ₁
Resolution (Å) ^a	50–3.4 (3.52–3.40)
Unit cell dimensions	
a, b, c (Å)	80.5, 80.5, 247.7
α, β, γ (°)	90, 90, 90
No. of measured reflections	112,326
No. of unique reflections	21,586
Redundancy	5.2 (5.4)
Completeness (%)	100 (100)
$\langle I/\sigma(I) \rangle$	25.2 (2.2)
R_{merge}	0.070 (0.593)
Wilson B-factor (Å ²)	120.1
Refinement statistics	
Resolution (Å)	49.0–3.40
$R_{\text{work}}/R_{\text{free}}$ (%)	28.0/33.0
Number of Molecules per asymmetric unit	2
Number of atoms	
Protein	7,114
Average B value (Å ²)	
Protein	135.1
R.m.s deviations	
Bond lengths (Å)	0.005
Bond angles (°)	0.834
Ramachandran plot	
Most favored (%)	88.9
Allowed (%)	10.3
Outliers	0.8

^aHighest shell data in parentheses.

MUN domain binds more specifically to the Munc18-1/Syx1 complex than isolated Syx1 and that the MUN domain promotes SNARE complex assembly starting from Syx1 bound to Munc18-1 but not from isolated Syx1 (Ma *et al.*, 2011; Yang *et al.*, 2015). It would be expected that the interplay between Munc18-1 and Munc13 in exocytosis reflects a general principle of SM proteins and their partner tethering complexes that contributes to most intracellular membrane fusion events (Laufman *et al.*, 2009; Wickner, 2010; Morgera *et al.*, 2012; James & Martin, 2013; Baker & Hughson, 2016).

Although the opening of the Syx1 linker region and the extension of domain 3a are required for MUN-catalyzed transition from the Munc18-1/Syx1 complex to the SNARE complex, however, the mechanism underlying the two conformational changes remains unclear. First, the smFRET data showed that the Syx1 linker region has an intrinsic tendency to assume a stably closed structure, and its conformational change (closed to open) is specifically driven by the MUN domain regardless of the conformational change of domain 3a (Figs 4 and 6). These data reinforce the notion that

Munc13 regulates exocytosis by neutralizing Syx1 autoinhibition (Wang *et al.*, 2017). Second, our ensemble FRET results suggest that the opening of the Syx1 linker region leads to the extension of domain 3a, but not *vice versa* (Fig 6). In line with this notion, the structural data reveal that domain 3a exhibits more conformational flexibility when Munc18-1 no longer binds to the closed Syx1 (Hu *et al.*, 2011; and Fig 7). Third, the observation that the MUN domain promotes the interaction between the Munc18-1/Syx1 complex and Syb2 (Fig 5) suggests that the MUN domain enables the extension of domain 3a via driving the opening of Syx1. Altogether, these results depict a coherent picture of how Munc13 and Munc18-1 act together to achieve the opening of Syx1 and the extension of domain 3a.

Our results (Fig 5) combined with those of previous studies (Parisotto *et al.*, 2014; Sitarska *et al.*, 2017; Jiao *et al.*, 2018) have demonstrated that L348 in the extended domain 3a mediates Syb2 binding. This binding, together with the interaction between Munc18-1 and Syx1-H3 (mediated by K332/K333 at the bottom of domain 3a, Fig 8) collectively suggests domain 3a constitutes the minimal unit responsible for associating both Syb2 and the open Syx1. According to this model, the binding site corresponding to K332/K333 in Syx1-H3 is located approximately at SNARE layer –4. This leads us to suspect that the N-terminal end of Syx1-H3 (layers –7 to –5) is not involved in binding to domain 3a, and this N-terminal end is likely to adopt a flexible conformation. In parallel, the N-terminal end of the SNARE motif of Syb2 is not involved in binding to domain 3a (Sitarska *et al.*, 2017; Jiao *et al.*, 2018). Hence, the N-terminally flexible regions of both Syb2 and Syx1-H3 would be available to accommodate SN25 entry, leading to N-terminal SNARE assembly. From a structural point of view, the tight association of most SNARE layers (layers –4 to +4) of Syx1-H3 within the Munc18-1/Syx1 complex would force SNARE assembly to proceed inside the central cavity of Munc18-1. Structural fluctuations of domains 1 and 3a allow the size of the central cavity of Munc18-1 to become narrower or wider (Fig 7, Bar-On *et al.*, 2011; Hu *et al.*, 2011; Baker *et al.*, 2013), with Habc becoming gradually detached while Syx1 becomes progressively more open during SNARE assembly. These lead to a hypothesis that Munc18-1 binds the SNARE four-helical bundle via its central cavity. In contrast, previous studies reported an alternative Munc18-1/SNARE complex binding mode, in which SNARE assembly proceeds with the extended domain 3a facing away the central cavity of Munc18-1 (Parisotto *et al.*, 2014; Yu *et al.*, 2018). Nevertheless, future investigations need to solve the structures of the intermediate assemblies and to determine which mode is more physiologically relevant.

Altogether, we investigated the analyzed mutations, their protein properties, and their sequential effects/performances in *in vitro* and *in vivo* assays (Table 2) and elucidated the mechanism underlying the roles of Munc18-1 and Munc13-1 in the early stage of vesicle priming. First, autoinhibitions of the Syx1 linker region and the Munc18-1 domain 3a inhibit the activity of the Munc18/Syx1 complex in SNARE assembly (Fig 9A). Second, the MUN domain binds to the Munc18-1/Syx1 complex to initiate the opening of the Syx1 linker region (Fig 9B), and as a consequence, the opening of the Syx1 linker region leads to the extension of domain 3a; the two conformational changes cooperate to activate the Munc18-1/Syx1 complex (Fig 9B). Third, the extended domain 3a in the activated complex primes Syb2 and Syx1, which further accelerates vesicle priming (Fig 9C). Fourth, the final entry of

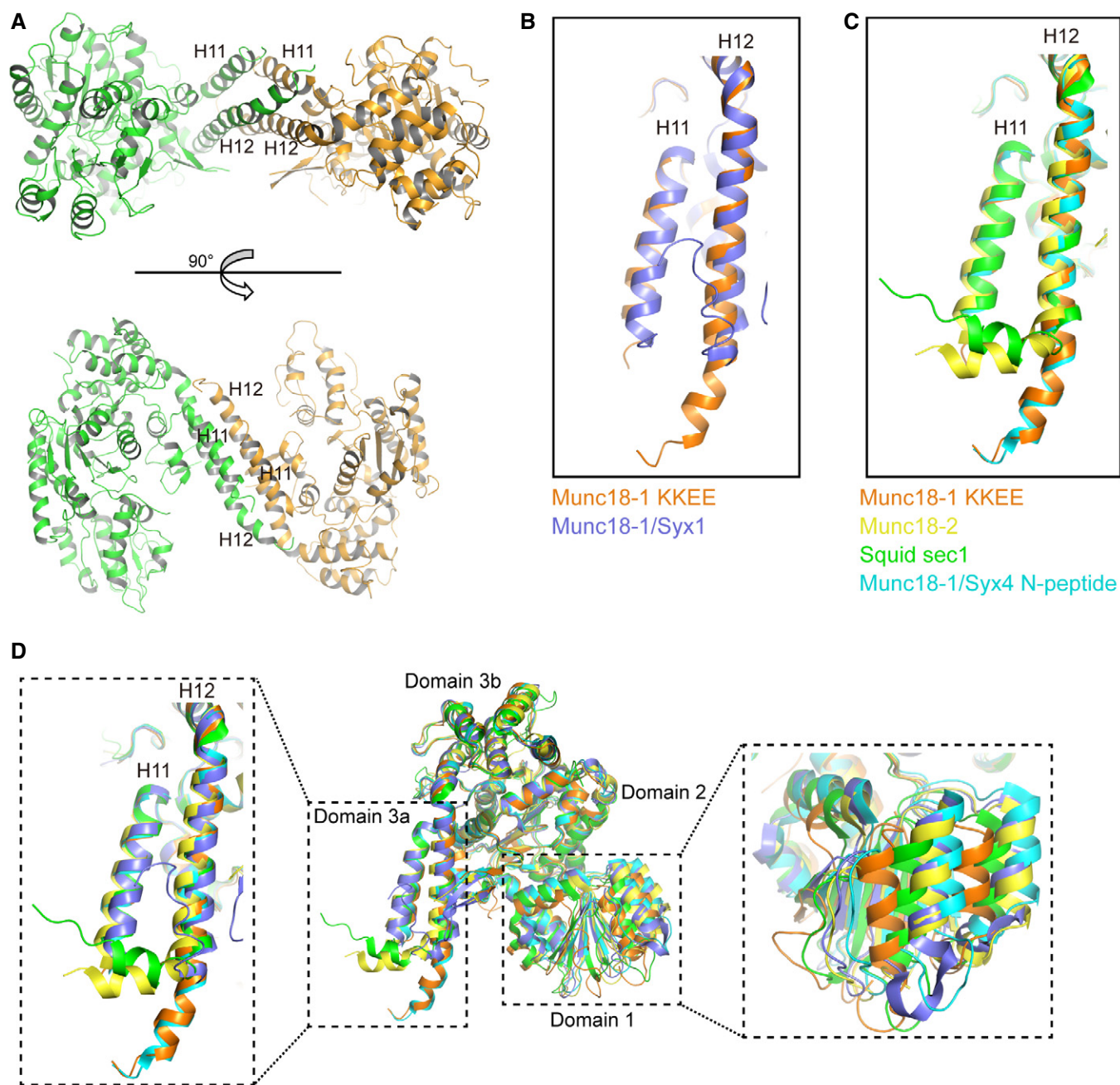


Figure 7. Crystal structure of Munc18-1 containing KKEE mutation.

A Ribbon diagrams of the structure of rat Munc18-1 containing the K332E/K333E mutation, two orientations rotating 90° with respect to each other were shown. Two Munc18-1 K332E/K333E molecules in an asymmetric unit pack against each other through helix–helix interaction in domain 3a.

B, C Structure alignment of domain 3a with various SM proteins. Crystal structure of domain 3a from rat Munc18-1 K332E/K333E was aligned and superposed with rat Munc18-1 WT in complex with closed Syx1 (pdb entry: 3C98) (B), and with human Munc18-2 (pdb entry:4CCA), nSec1 from squid (pdb entry:1FVH), and rat Munc18-1 WT in complex with mouse Syx4 N-peptide (pdb entry: 3PUJ) (C).

D The flexibility of SM proteins in domain 3a and domain 1. Structures of rat Munc18-1 WT in complex with closed Syx1, human Munc18-2, nSec1 from squid, and rat Munc18-1 WT in complex with mouse Syx4 N-peptide were aligned and superposed with rat Munc18-1 K332E/K333E. Enlarged views of domain 3a and domain 1 are shown in dashed boxes.

Data information: Color codes are as follows: Munc18-1 (KKEE), orange; Munc18-1/Syx1, slate blue; human Munc18-2, yellow; nSec1 from squid, green; Munc18-1/Syx4 N-peptide, cyan.

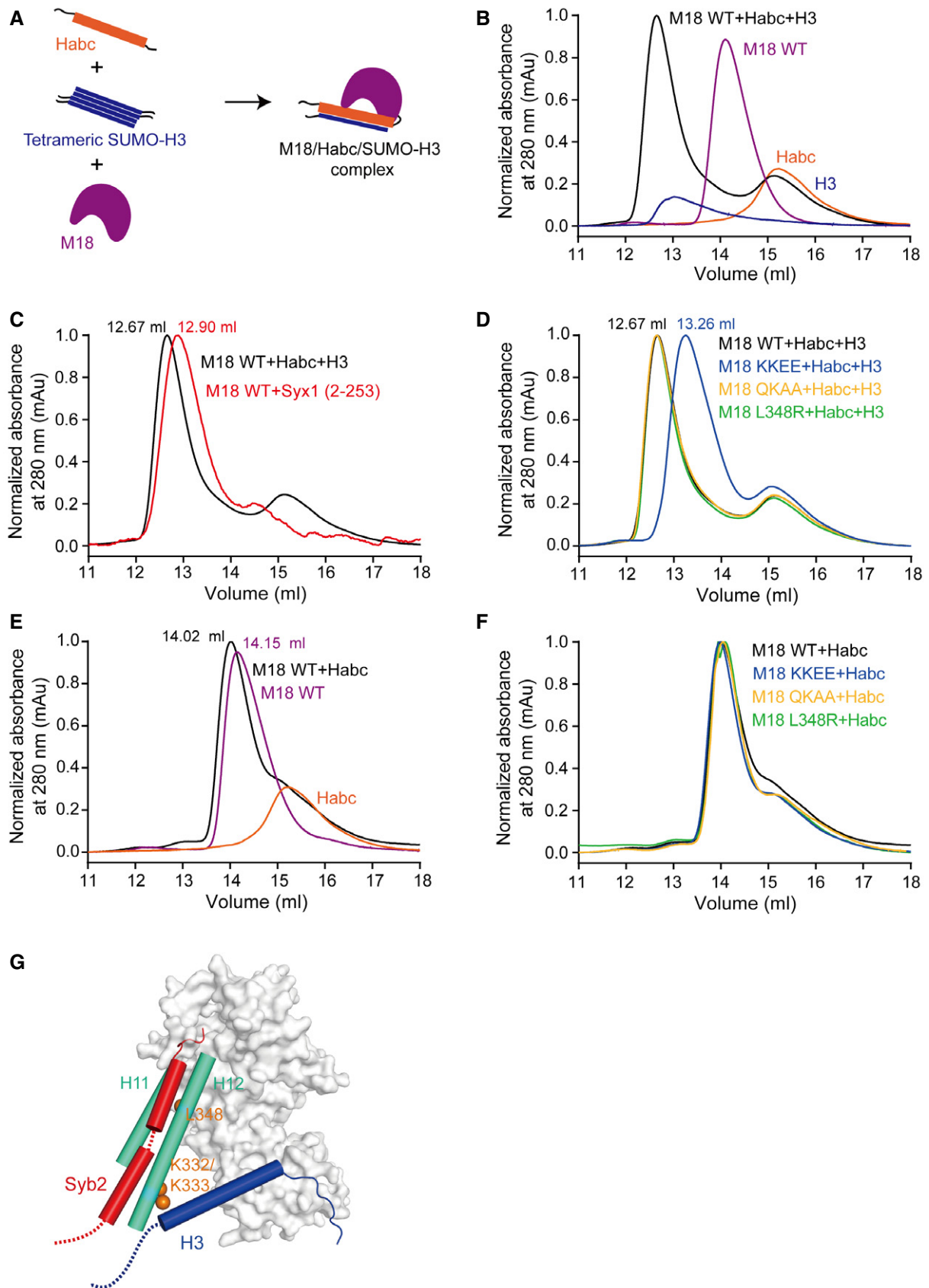
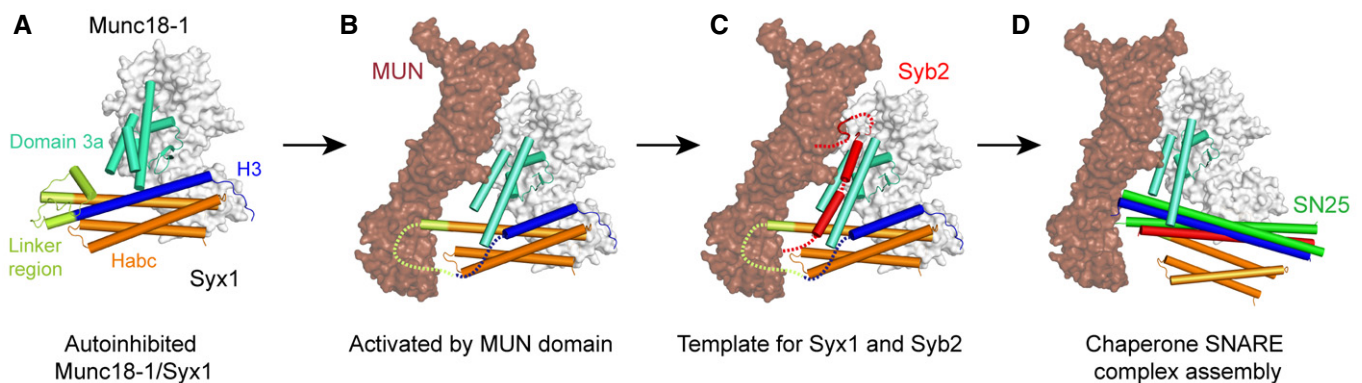


Figure 8.

Figure 8. The Munc18-1 domain 3a constitutes a minimal template for Syx1 and Syb2.

- A Schematic depiction of a putatively tertiary Munc18-1/Habc/H3 complex.
 B Munc18-1, Habc, and H3 construct a tertiary complex.
 C The tertiary complex globally resembles the Munc18-1/Syx1 complex.
 D Formation of the tertiary complex with Munc18-1 QKAA, KKEE, and L348R mutants. KKEE strongly impaired formation of the tertiary complex.
 E Munc18-1 displays interaction with Syx1-Habc.
 F QKAA, KKEE, and L348R all retained interaction with Syx1-Habc.
 G Cartoon illustration of the templating mechanism of domain 3a. The extended domain 3a (H11 and H12) binds to Syx1-H3 and Syb2 simultaneously. Color codes are as follows: Munc18-1, light gray; Munc18-1 H11 and H12, cyan; Syx1-H3, blue; Syb2, red. Key binding sites (L348, K332, and K333) on the H12 are highlighted with orange spheres.

Data information: All the proteins or protein complexes were analyzed on a Superdex 200 Increase 10/300 GL size-exclusion column.

**Figure 9. Model of Munc18-1 and Munc13 in driving SNARE assembly.**

- A Autoinhibition of the Munc18-1/Syx1 complex. The closed Syx1 linker region and the bent Munc18-1 domain 3a render this complex inactive, inhibiting Syx1 association with SN25 and Syb2.
 B Activation of the Munc18-1/Syx1 complex by Munc13 MUN domain. The MUN domain catalyzes opening of the Syx1 linker region via binding to H11 of domain 3a and Syx1 linker region, leading to a conformational flexibility of domain 3a (between bend and extension). The open Syx1 linker region and putative unstructured N-terminal of Syx1-H3 are displayed by lemon green and blue dashed lines, respectively.
 C Templating function of domain 3a. Assisted with Munc13 MUN domain, the extended domain 3a serves as a template for Syx1-H3 and Syb2 simultaneously, awaiting SN25 entry and registering SNARE complex assembly at the N-terminus. Dashed lines indicate putative unstructured regions.
 D SNARE complex assembly. Proceeding of SNARE four-helix bundle inside the central cavity of Munc18-1 to complete SNARE complex formation and membrane fusion.

Data information: Color codes are as follows: Munc18-1, light gray; the Munc18-1 domain 3a, cyan; Syx1-Habc, orange; Syx1 linker region, lemon green; Syx1-H3, blue; Munc13-1 MUN domain, brown; Syb2, red; SN25, green.

SN25 initiates N-terminal SNARE assembly, and the formation of the SNARE four-helical bundle likely proceeds inside the central cavity of Munc18-1 (Fig 9D).

According to the Vps33/Vam3 and Vps33/Nyv1 binding modes (Baker *et al*, 2015), vesicle priming requires Munc18-1 to serve as a template to allow Syb2 and Syx1 to associate (Parisotto *et al*, 2014; Baker *et al*, 2015; Sitariska *et al*, 2017; Jiao *et al*, 2018). More recent studies have revealed that Munc18-1 and Munc13 cooperate to form a well-defined template for ensuring proper SNARE assembly (Wang *et al*, 2019; Shu *et al*, 2020), in a fashion resistant to disassembly by NSF/ α -SNAP (Ma *et al*, 2013; He *et al*, 2017; Lai *et al*, 2017; Stepien *et al*, 2019). In this study, we propose that a quadruple MUN/Syb2/Munc18-1/Syx1 complex likely represents an intermediate during SNARE complex formation (Fig 9C). Multiple interactions are involved in this quadruple complex: (i) Syb2 interacts with domain 3a via its SNARE motif and with the MUN domain via its membrane-proximal region (Parisotto *et al*, 2014; Baker *et al*, 2015;

Wang *et al*, 2019); (ii) Syx1 binds to Munc18-1 via its H3 and Habc domains, and to the MUN domain via the linker region (Misura *et al*, 2000; Yang *et al*, 2015; Wang *et al*, 2017); and (iii) Syx1-bound Munc18-1 binds the MUN domain via domain 3a (via Q301/K308 in helix H11). The finding of the multiple and reciprocal interplay among Munc18-1, Munc13, Syx1, and Syb2 sheds new light on the way in which SM proteins, tethering factors, and SNAREs cooperate to achieve regulated membrane fusion.

Materials and Methods

Plasmid constructions

Full-length rat Munc18-1 (residues 1–594), rat Syt1 cytoplasmic domain C2AB (residues 140–421), and SNARE motifs of human SN25 (SN1, residues 11–82; and SN2, residues 141–203) were

cloned into pGEX-KG vector that includes an N-terminal thrombin cleavable GST tag. Full-length rat Syb2 (residues 1–116) and its cytoplasmic domain (residues 29–93), and rat Syx1 cytoplasmic fragment (residues 2–253) were cloned into pGEX-6P-1 vector. Full-length human SN25 (with its four cysteines mutated to serines), C-terminal 6 × His-tagged Syx1 (residues 2–253, with ternary mutations of S95C/C145S/S171C), rat Munc13-1 MUN domain (residues 933–1,407, EF, 1,453–1,531), and Syx1 Habc domain (1–180) were constructed into pET28a vector (Novagen). The Syx1 SNARE motif (H3, residues 191–253) was cloned into pET-SUMO vector (Invitrogen). WT Munc18-1/Syx1 (residues 1–288), Munc18-1/Syx1 (residues 2–253), and their mutants were constructed into pETDuet-1 vector (Novagen). All mutations were generated with Site-Directed Mutagenesis Kit (Stratagene) from the corresponding wild-type fragments. Rat Munc13-1 C1-C2B-MUN fragment (residues 529–1,407, EF, 1,453–1,531) was cloned into pFastBacTMHT B vector (Invitrogen) and expressed in insect cells (Sf9) derived from *Spodoptera frugiperda* as previously described (Ma et al, 2013).

For *in vivo* imaging assays, Munc18-1 and Syx1 cDNA sequences were subcloned within vectors pEGFP-C1 (Clontech) and mCherry2-C1 (Addgene), respectively, all into *EcoRI/SalI* sites of the vectors. Enhanced green fluorescent protein (EGFP) and mCherry2 protein serving as indicators of transfected cells were co-expressed with Munc18-1 and Syx1, respectively.

To knock down the expression of Munc18-1 in primary cultured mouse cortex neurons, we expressed short hairpin RNA (shRNA) to silence the expression of Munc18-1. A 6-nucleotide sequence (CCATGG) was used as a linker to connect inverted repeated nucleotide sequences (GTCTGTCCACTCTCATC) (Arunachalam et al, 2008). We performed annealing step to generate 55 base-pair oligonucleotides containing sense and anti-sense of the target sequences. Next, the oligonucleotides were introduced into a lentiviral vector (L309) digested by restriction enzymes *XhoI* and *XbaI* downstream of H1 promoter. Munc18-1 WT and mutant sequences were inserted into the *BamHI/EcoRI* sites downstream of the UbC promoter. To protect mRNA transcripts transcribed from the Munc18-1 rescued plasmids from being degraded, five silent nucleotide mutations were introduced into Munc18-1 gene (G246A, T249C, C255T, T258C, and C264T). For overexpression of Munc18-1 in WT background neurons, Munc18-1 WT and mutant sequences were inserted into the *BamHI/EcoRI* sites downstream of the UbC promoter of L309 vector directly.

Recombinant protein expression and purification

All recombinant proteins except for Munc13-1 C1C2BMUN fragment were expressed in *Escherichia coli* BL21 (DE3) with growing cells to an optimal density at 600 nm (OD₆₀₀) of 0.8 at 37°C and induced by 0.4–0.5 mM isopropyl-β-D-thiogalactoside (IPTG) at 16°C or 20°C. All proteins were purified as described previously (Ma et al, 2013; Yang et al, 2015; Wang et al, 2017). In brief, GST-fused proteins bound to glutathione Sepharose 4B (GE Healthcare) affinity media were digested by thrombin and GST-fused PreScission Protease or eluted with 20 mM reduced L-glutathione for GST pull-down experiments. Eluted proteins were loaded onto size-exclusion chromatography system (GE Healthcare) for further purification. Hexahistidine-tagged proteins bound to Nickel-NTA agarose affinity

media (Qiagen) were eluted with buffer containing 300 mM imidazole and further purified by size-exclusion chromatography.

For Munc18-1 purification, cultured cells were harvested by centrifuging at 5,000 g with a JS-4.2 rotor (Beckman Coulter) for 20 min at 4°C and re-suspended in phosphate-buffered saline (PBS) at pH 7.4. Cells were lysed by an AH-1500 Nano Homogenize Machine (ATS Engineering Inc.) with PBS buffer supplied with 1 mM phenylmethanesulfonyl fluoride (PMSF, Amresco), 5 mM 1,4-dithio-DL-threitol (DTT), and 1 mM EDTA (with pH adjustment to 8.0 by NaOH) for three times at 800–1,000 bar at 4°C. Supernatants were separated after centrifuging at 31,000 g in a JA-25.50 rotor (Beckman Coulter) at 4°C for 30 min. GST-Munc18-1 supernatants were incubated with glutathione Sepharose 4B affinity media, rotating for 3 h at 4°C. The bead-bound proteins were washed extensively with buffer containing 20 mM Tris-HCl (pH 8.0), 1 M NaCl, 10% (v/v) glycerol, and 5 mM DTT. For removing GST tag, 10 U/ml of thrombin was incubated with media in buffer T (20 mM Tris-HCl (pH 8.0), 150 mM NaCl, 10% (v/v) glycerol, and 5 mM DTT) overnight at 4°C. Further purification was performed on a Superdex 200 16/600 column (GE Healthcare).

Native-PAGE assay

Purified Munc18-1 were incubated with Syx1 (residues 2–253) with a protein-to-protein ratio of 1.2:1 overnight at 4°C to form Munc18-1/Syx1 complex efficiently. Then, Munc18-1/Syx1 complex was mixed with the Syb2 (29–93) and SN25 in the absence or presence of Munc13-1 MUN domain at 30°C for 2 h (final concentration of proteins: Munc18-1/Syx1, 3 μM/2.5 μM; Syb2 and SN25, 10 μM; MUN domain, 30 μM). 8 μl samples were mixed with 2 μl 5 × native loading buffer and injected into the well of 15% non-denaturing polyacrylamide gel (native gel). Native gel was prepared without SDS to maintain the activity of proteins. Subsequently, electrophoresis was carried out with constant current 20 mA per gel at 4°C for 2 h. Gels were stained with Coomassie Brilliant Blue, and bands of Munc18-1/Syx1 were quantified with ImageJ (NIH).

Ensemble FRET experiment

Syb2 (residues 29–93, with mutation of S61C) and SN25 (with native cysteines mutated to serines and Q197C mutation) were labeled with donor-dye BODIPY FL-maleimide (Molecular Probes) and acceptor-dye tetramethylrhodamine-5-maleimide, single isomer (TMR, Molecular Probes) respectively. Purified proteins were mixed with dyes with a protein-to-dye ratio of 1:5 in buffer H (25 mM HEPES (4-(2-hydroxyethyl)-1-piperazineethanesulfonic acid) pH 7.4, 150 mM KCl, 10% glycerol (v/v)), gently rotated overnight at 4°C in the dark. The reactions were stopped with addition of 10 mM DTT, and excess dyes were removed using PD-10 desalting columns (GE Healthcare) with buffer H. To monitoring the transition of Munc18-1/Syx1 complex to the SNARE complex by Munc13-1 MUN domain, co-expressed Munc18-1/Syx1 (2–253) WT or mutants with final concentration of 10 μM were mixed with 10 μM TMR-labeled SN25 and 2 μM BODIPY FL-labeled Syb2 in the absence or presence of 30 μM MUN domain. For monitoring the transition of Munc18-1/Syx1 with Syx1 LEAA mutation or Munc18-1 P335A mutation to the SNARE complex, Munc18-1 and Syx1 were pre-incubated with a ratio of 1.5:1 at 4°C overnight to form Munc18-1/Syx1 complex

Table 2. Summary of functional performance of Munc18-1 mutants in various assays.

M18/Syx complex Function analysis	WT	Q301A/K308A	K332E/K333E	P335A	L348R
MUN-catalyzed transition to the SNARE complex (native PAGE)	+	–	–	+	–
MUN-catalyzed transition to the SNARE complex (FRET)	+	–	–	+	–
Liposome fusion (lipid mixing)	+	–	–	N/A	–
Synaptic vesicle exocytosis (cellular electrophysiology)	+	–	–	+	–
M18 and Syx1 transport (confocal imaging)	+	+	+	N/A	+
Interaction with Syx1 (GST pull-down)	+	+	+	N/A	+
Opening Syx1 linker region (single-molecule FRET)	+	–	+	+	+
Interaction with Syb2 in the presence of MUN (GST pull-down)	+	–	+	+	–
Formation of M18-1/H3/Habc complex (gel filtration)	+	+	–	N/A	+
Interaction with the assembled SNARE complex (GST pull-down)	+	+	+	N/A	+

+, positive; –, negative; N/A, not applicable.

efficiently. 5 μ M Munc18-1/Syx1 complex was mixed with 5 μ M TMR-labeled SN25 and 2 μ M BODIPY FL-labeled Syb2 with or without 20 μ M MUN domain. All ensemble FRET assays were performed by a QM40 spectrofluorometer (Photon Technology Incorporated) with an excitation wavelength of 485 nm and monitored an emission wavelength at 513 nm at 30°C in 1-cm quartz cuvette. FRET efficiency was analyzed with the formula: $E = (F_0 - F_{obs})/F_0 \times 100\%$ (E : FRET efficiency; F_0 : the initial fluorescent intensity; F_{obs} : the observed fluorescent intensity). Each experiment was repeated at least three times.

Liposome fusion assay

Lipid powders (all obtained from Avanti Polar Lipids) were dissolved with chloroform at final concentration of 10 mg/ml, except for PIP2 was dissolved in a mixture of chloroform:methanol:

water (20:9:1) at concentration of 1 mg/ml. All lipids were stored at –20°C. Lipid mixtures were dried with nitrogen gas and further incubated in vacuum for at least 3 h at room temperature in the dark. Lipid films were re-suspended in buffer H supplied with 0.2 mM Tris(2-Tris (2-carboxyethyl)phosphine (TCEP, Sigma-Aldrich) and 1% CHAPS (*w/v*, Amresco). For lipid-mixing assays using Munc18-1/Syx1 liposomes, lipids were mixed at the proper ratio as indicated below with total lipid to a final concentration of 5 mM. Donor liposomes (*v*-liposome, reconstituted with Syb2 (residues 1–116)) contain 60% POPC, 17% POPE, 20% DOPS, 1.5% NBD-PE, 1.5% Rhodamine-PE, and acceptor liposomes (*t*-liposome, reconstituted with Munc18-1/Syx1 (residues 1–288)) contain 58% POPC, 15% POPE, 20% DOPS, 2% PIP2, and 5% DAG. Purified proteins were added with protein-to-lipid ratio of 1:500 for *v*-liposomes and 1:1,000 for *t*-liposomes, respectively. After incubation on the ice for 1 h, lipid–protein mixtures were dialyzed against buffer H supplied with 1 mM DTT three times at 4°C, and 1 g/l Bio-Beads SM2 (Bio-Rad) was added at the last time to remove the detergent extensively. The *v*-liposomes (0.25 mM lipids) were mixed with *t*-liposomes (0.5 mM lipids) in a total volume of 60 μ l in the presence of 2 μ M Syt1 C2AB fragment, 1 mM Ca^{2+} , with or without 5 μ M SN25, and with or without 1 μ M C1-C2B-MUN (as indicated in the figure charts). All lipid-mixing assays were carried out at 30°C in a 1-cm quartz cuvette and monitored by measuring donor (NBD: emission at 538 nm; excitation at 460 nm) fluorescence using a QM-40 spectrophotometer. Raw data were normalized to the fluorescence intensity after addition of 6 μ l 10% CHAPS (*w/v*). Each experiment was repeated at least three times.

GST pull-down assay

For monitoring the interaction between Syx1 and Munc18-1, 3 μ M N-terminal GST-tagged Syx1 (2–253) and 6 μ M Munc18-1 WT or mutants were incubated with 10 μ l glutathione Sepharose 4B affinity media in a final volume of 100 μ l in buffer H. The mixtures were gently rotated at 4°C for 2 h. After being washed extensively with buffer H for three times, SDS-loading buffer was added and samples were then boiled at 100°C for 10 min and analyzed by SDS-PAGE followed by Coomassie Brilliant Blue staining.

For detecting the interaction between Munc18-1/Syx1 and Munc13-1 MUN domain, 5 μ M GST-Syx1 (residues 2–253) was immobilized on glutathione Sepharose 4B affinity media and incubated with 6 μ M Munc18-1 to form Munc18-1/Syx1 complex for 2 h at 4°C. 10 μ M MUN domain (recombined with hexa-histidine tag for immunoblotting) was added to the mixture to a final volume of 100 μ l with buffer H. After gently shaking for 3 h at 4°C, the samples were washed 3 times using buffer H and analyzed with SDS-PAGE followed by immunoblotting using 6 \times His-tag mouse monoclonal antibody (Proteintech #66005-1-Ig) and GST-tag rabbit polyclonal antibody (Proteintech #10000-0-AP).

For monitoring the interaction between Syb2 and Munc18-1/Syx1 in the presence or absence of MUN domain, Munc18-1 WT or mutants were pre-incubated with Syx1, respectively, with a protein-to-protein ratio of 1:1.5 overnight at 4°C to form Munc18-1/Syx1 sufficiently. 3 μ M GST-Syb2, 5 μ M Munc18-1/Syx1, and 10 μ M MUN domain (if applicable) were mixed with 10 μ l glutathione Sepharose 4B affinity media to a final volume of 100 μ l in buffer H containing 0.05% Triton X-100 (*v/v*). After gentle rotation for 4 h at

4°C, beads were washed three times with buffer H. Samples were analyzed by SDS-PAGE, and the quantification of Munc18-1 bands was acquired by ImageJ (NIH).

For detecting the interaction between Syb2 and Munc18-1, 2 μM GST-Syb2 and 5 μM Munc18-1 WT or mutants were incubated with 10 μl glutathione Sepharose 4B affinity media in a final volume of 100 μl in buffer H. After gently shaking for 3 h at 4°C, samples were washed three times using buffer H and analyzed with SDS-PAGE followed by Coomassie Brilliant Blue staining.

To detect the interaction between Munc18-1 and SNARE complex, SNARE complex was prepared with 5 μM GST-SN1, 6 μM SN2, 6 μM Syb2 (residues 29–93), and 5 μM Syx1 (residues 2–253) and incubated with 10 μl glutathione Sepharose 4B affinity media overnight at 4°C. Beads were washed with buffer H to remove the excess proteins. 10 μM purified Munc18-1 WT and mutants were added to the mixture and incubated at 4°C for 4 h. Extensive washing was performed with buffer H. Samples were analyzed by SDS-PAGE followed by Coomassie Brilliant Blue staining.

Analytical size-exclusion chromatography

To identify formation of Munc18-1/Habc/H3 and Munc18-1/Habc complex, 12 μM Munc18-1 and 120 μM Syx1 Habc domain were mixed in the presence or absence of 60 μM SUMO-H3 in a total volume of 200 μl in buffer H. To detect the binding of Munc18-1/H3 or Habc/H3 complex, 60 μM SUMO-H3 was mixed with 12 μM Munc18-1 or 120 μM Syx1 Habc domain in a total volume of 200 μl in buffer H. Samples were incubated at 16°C for 4 h and loaded onto a Superdex 200 Increase 10/300 GL size-exclusion column. All experiments were performed on AKTA pure (GE Healthcare).

SNARE complex formation with the Munc18-1/Habc/H3 complex

To detect SNARE complex assembly from the Munc18-1/Habc/H3 complex, 2 μM Munc18-1/Habc/H3 complex, 5 μM SN1, 5 μM SN2, and 10 μM Syb2 were mixed in a total volume of 10 μl in buffer H at 30°C for 1 h. Samples were analyzed by SDS-PAGE followed by Coomassie Brilliant Blue staining.

Protein crystallization, data collection, and structure determination

Purified Munc18-1 K332E/K333E protein in buffer 20 mM Tris-HCl pH 8.0, 100 mM NaCl, 5 mM DTT was concentrated to 12 mg/ml for crystal screen. Crystallization trays were set up using the vapor diffusion method at 16°C with the hanging drop by mixing protein with an equal volume of reservoir solution. Crystals were grown in 4 M ammonium acetate, 0.1 M sodium acetate trihydrate pH 4.6, and grew to full size after 24 h. Before flash-freezing in liquid nitrogen, crystals were soaked in cryo-protection buffer containing 20% glycerol (*v/v*) for 30 s. All diffraction data were collected on beamline BL18U (Shanghai Synchrotron Radiation Facility) at 100 K. The data sets were processed with HKL3000 (HKL Research, Inc.). The primary structure of Munc18-1 K332E/K333E was determined by molecular replacement using the Phaser (McCoy *et al.*, 2007). The structure of Munc18-1 bound to Syx4 N-peptide (PDB ID code 3PUJ, chain A) was used as the starting model. The missing residues were built manually with Coot (Emsley *et al.*, 2010) according to $|F_o| - |$

$F_c|$ and $2|F_o| - |F_c|$ maps. Then, the refinement was carried out with phenix refinement program. Structure graphics were prepared using Pymol (Schroödinger).

Single-molecule FRET experiment (smFRET)

Standard procedure has been described elsewhere (Wang *et al.*, 2017). Homemade chamber for total internal reflection (TIR) smFRET contains a 25 × 75-mm size, 1-mm-thick glass slide and a 24 × 50-mm size, 0.13–0.16-mm-thick glass coverslip. A number of holes on the slide were drilled by 0.8 mm diamond drill to make four channels for each chamber (Diao *et al.*, 2012). The coverslips and drilled slides were first washed by sonication in 5% Alconox (Aldrich) for 30 min at 60 W power followed by sonication in acetone for additional 10 min and 1 M NaOH for 1 h at a power of 60 W. After extensively rinsing by deionized water, the slides and coverslips were soaked into methanol followed by burning on an alcohol burner to extinct any potential organic chromophores. Cleaned slides and coverslips were stored at room temperature in 50-ml centrifuge tubes before using.

Siliconization of the slides and coverslips were achieved by incubating in 100 ml methanol, 5 ml acetic acid, and 1 ml N-[3-(trimethoxysilyl)propyl]ethylenediamine (Aladdin) for 20 min in the dark. After extensive washing with deionized water and drying under nitrogen flow, the slides and coverslips were modified with mPEG-succinimidyl valerate, MW 5,000 (mPEG-SVA, Laysan Bio), and succinimidyl valerate-mPEG-succinimidyl valerate, MW 5,000 (SVA-PEG-SVA, Laysan Bio) dissolved in 0.1 M NaHCO₃ with a ratio of 9:1. Another round of modification using HBS7.6 (25 mM HEPES-K⁺ pH 7.6, 150 mM KCl) dissolved N_α,N_α-bis(carboxymethyl)-L-lysine (Sigma-Aldrich) was also included in order to immobilize hexa-histidine-tagged proteins. Modified slides and coverslips were rinsed with deionized water, dried under nitrogen flow, and stored at room temperature in 50-ml centrifuge tubes with nitrogen as blanket gas.

The imaging chamber contains a pair of slide and coverslip. The double-sided sticky tape was used as spacers for each channel. The chamber was finally sealed by epoxy. For the purpose of hexa-histidine-tagged protein immobilization, each channel was first activated by 0.5 M NaOH, followed by extensive washing with TBS300 (20 mM Tris-HCl pH 8.5, 300 mM NaCl). To increase the specificity, CoCl₂ (Sigma-Aldrich) was applied as chelated metal ions. All smFRET measurements were performed in imaging buffer (25 mM HEPES-K⁺ 150 mM KCl, supplied with oxygen scavenger (20 units/ml glucose oxidase (from *Aspergillus niger*, Sigma-Aldrich), 1,000 units/ml catalase (from bovine liver, Sigma-Aldrich), and 1% (*w/v*) glucose) to minimize photobleaching.

Purified Syx1 (S95C/C145S/S171C) were labeled stochastically with Alexa Fluor 555 C2 maleimide and Alexa Fluor 647 C2 maleimide (both from Invitrogen) with a protein-to-dye ratio of 1:5 in buffer H, gently rotated overnight at 4°C in the dark. Free dyes were removed using PD-10 desalting columns with buffer H. Munc18-1/Syx1 complex was prepared by mixing purified Munc18-1 and fluorescent-labeled Syx1 with a molar ratio of 2:1 at 4°C overnight. During the experiment, Syx1 was diluted to a final concentration of 0.5 μM and loaded into the imaging chamber. After incubation for 30 min at room temperature, the imaging buffer was used to wash out remnant unbound proteins. For experiments using double-labeled Syx1, 10 μM SN25,

10 μM Syb2, and/or 30 μM Munc13-1 MUN domain were added as indicated in the figure charts or legends.

Total internal reflection (TIR) imaging was achieved by using a $100\times$ TIRF objective (NA 1.49, Nikon) on a Nikon Ti2 inverted microscope equipped with an electronic motored TIRF illuminator, a beam splitter with Cy3/Cy5 filter cube (Carin-Research OptoSplit II), an EMCCD camera (Andor iXon DU987), and a Sapphire 532 LP (100 mW, Coherent) solid-state laser. Image acquisition was achieved by the software Single (version 0.4, by Taekjip Ha, <http://ha.med.jhmi.edu/resources/>). The exposure time for each frame was set to 100 ms and 200 frames were acquired for each observed fields. IDL 8.2 (Exelis Visual Information Solutions) and MATLAB R2010b (MathWorks) were used for data processing and analysis, and source codes are from Taekjip Ha's smFRET data analysis package.

Confocal imaging

HEK293T cells (CRL-11268, ATCC) were grown at 37°C and 5% CO_2 in a humidified atmosphere incubator (Thermo). The culture medium contained Dulbecco's modified Eagle's medium (Gibco), 10% fetal bovine serum, and penicillin-streptomycin (50 and 50 $\mu\text{g}/\text{ml}$). After being cultured in glass-bottom dishes (NEST, 801001) for 12 h, HEK293T cells were transfected or co-transfected with EGFP-Munc18-1 or/and mCherry2-Syx1. Lipophilic dye DiD (Invitrogen, D7757, 10 mM in ethanol) was diluted to the cell suspension (in DMEM) to a final concentration of 10 μM . After an incubation of 20 min at 37°C , cells were washed twice with PBS and kept in the dark at room temperature until analysis. Images were acquired by using a Nikon C2 confocal microscope equipped with a $60\times$ oil-immersion objective after cells were transfected for 24 h. For statistical calculation, we obtained the interception pictures (using Adobe Photoshop CS6 software) of cells that were both expressed EGFP-Munc18-1 and mCherry2-Syx1 and marked with DiD. One interception picture contains one to three intact cells. Our statistical results are derived from further data processing of these cell interception pictures. Image detection and segmentation were achieved by using home-written MATLAB scripts (version 2010b). In brief, the script detects DiD-positive region as plasma membrane (PM) and makes a mask for detecting EGFP-Munc18-1 and mCherry2-Syx1 on plasma membrane. Next, using morphological processing, the PM-mask is filled as total cell-mask (Total) for detecting EGFP-Munc18-1 and mCherry2-Syx1 in total cell. Finally, the fluorescent intensities of EGFP-Munc18-1 and mCherry2-Syx1 are integrated according to the masks. The PM-distribution ratio is given by:

$$r_{(\text{PM}/\text{Total})} = \frac{I_{\text{PM}}}{I_{\text{Total}}}$$

where I represents the integrated fluorescent intensity of EGFP or mCherry2; PM, plasma membrane. The source MATLAB script for data processing is available upon requisitions.

Neuron culture

The dissociated cortical neurons were prepared from P0 pups, as described previously (Wang *et al*, 2017). Briefly, mouse cortex were

dissociated from postnatal day 0 (P0) of WT mice, dissociated by 0.25% trypsin digestion for 12 min at 37°C , plated at a density of 80,000 per circular glass coverslips (12 mm diameter) coated with poly-L-lysine (Sigma), and cultured in MEM (GIBCO) supplemented with 2% (v/v) B27 (GIBCO), 0.5% (w/v) glucose, 100 mg/l transferrin, 5% (v/v) fetal bovine serum, and 2 mM Ara-C (Sigma). Neurons were grown at 37°C , 5% CO_2 in a cell incubator (Thermo).

All animal procedures were performed in accordance with South-Central University for Nationalities animal use rules and the requisite approvals of animal use committees.

Lentiviruses preparation

Lentiviral expression vectors and three helper plasmids (pRSV-REV, pMDLg/pRRE, and pVSVG) were co-transfected into HEK293T cells. The transfections were carried out using the polyethylenimine (PEI) method with the ratio at PEI:pFUGW:pVSVG:pRRE:REV = 24:3:1:2:2. The virus-containing medium was harvested at 48 hours after transfection and subsequently pre-cleaned with a 1,000 g centrifuge and a 0.45 μm filtration (Millipore). The virus-containing medium was overlaid on a sucrose-containing buffer (50 mM Tris-HCl pH 7.4, 100 mM NaCl, 0.5 mM EDTA) at a 4:1 (v/v) ratio and centrifuged at the indicated RCF at 4°C . After centrifugation, the supernatant was carefully removed, and the tube was placed on the tissue paper for 3 min. PBS buffer was added to the semi-dried tube for re-suspension, and then, the tube was placed in the 4°C fridge with a cover for recovery overnight. All steps were performed under level II biosafety conditions. Neurons were infected with lentiviruses at days *in vitro* (DIV) 4–6 and electrophysiological analyzed at DIV 13–14.

The expression of Munc18-1 and its mutants in neurons at DIV 13–14 was quantitated by Western blotting using Munc18-1 antibody (rabbit polyclonal antibody, Proteintech #11459-1-AP).

Electrophysiological recordings

Electrophysiological recordings were performed in whole-cell patch-clamp mode using concentric extracellular stimulation electrodes as described previously (Wang *et al*, 2019). Patch pipettes were pulled from borosilicate glass capillary tubes (World Precision Instruments, Inc.) using a P-97 pipette puller (Sutter). The resistance of pipettes filled with intracellular solution varied between 3 and 5 MOhm. The whole-cell pipette solution contained 120 mM CsCl, 10 mM HEPES, 10 mM EGTA, 0.3 mM Na-GTP, 3 mM Mg-ATP, and 5 mM QX-314 (pH 7.2, adjusted with CsOH). The bath solution contained 140 mM NaCl, 5 mM KCl, 2 mM MgCl_2 , 2 mM CaCl_2 , 10 mM HEPES-NaOH, and 10 mM glucose (pH 7.4). IPSCs were pharmacologically isolated by adding the AMPA and NMDA receptor blockers CNQX (20 μM) and AP-5 (50 μM) to the extracellular solution. AP-5 (50 μM) and the GABAA-receptor blockers picrotoxin (100 μM) were added to the extracellular solution to isolate EPSCs. Synaptic currents were monitored with an EPC10 amplifier (HEKA). Spontaneous mIPSCs and mEPSC were monitored in the presence of tetrodotoxin (TTX, 1 μM) to block action potentials. Miniature events were analyzed in Clampfit 10 (Molecular Devices) using the template matching search and a minimum threshold of 5 pA and each event was visually inspected for inclusion or rejection by an experimenter blind to the recording condition. Single extracellular stimulus pulses (90 μA ,

1 ms) were controlled with a Model 2100 Isolated Pulse Stimulator (A-M Systems, Inc.) for all evoked IPSCs measurements. The evoked IPSCs were monitored in the addition of 50 μ M AP-5 and 20 μ M CNQX to the bath solution. The sucrose-evoked release was triggered by a 30-s application of 0.5 M sucrose to the bath solution which also contained AP-5, CNQX, and TTX. All data were analyzed in Clampfit 10 (Molecular Devices).

Immunostaining

Mouse cortical neurons infected with various lentiviruses were fixed in 4% paraformaldehyde and permeabilized with 0.2% Triton X-100, incubated with anti-Munc18-1 (rabbit polyclonal antibody, Proteintech #11459-1-AP), and anti-synapsin1 (mouse monoclonal, Santa Cruz # sc-398849) primary antibodies in PBS with 5% BSA, washed, and visualized using Alexa Fluor-488 goat anti-mouse and Alexa Fluor-546 goat anti-rabbit secondary antibodies (Molecular Probes). Primary antibodies anti-synapsin1 were used to mark synapse. Images were acquired by using a Nikon C2 confocal microscope equipped with a 60 \times oil-immersion objective. Identical settings were applied to all samples in each experiment. Synapse size and number were analyzed by ImageJ (NIH).

Statistical analysis

Prism 6.01 (GraphPad) was used for statistical tests, all of which are described in figure legends.

Data availability

The crystal structure of rat Munc18-1 with K332E/K333E mutation solved in this study is available in Protein Data Bank (PDB, [http://www.wwpdb.org](http://www ww p d b . o r g)) with an accession code of 6LPC.

Expanded View for this article is available online.

Acknowledgements

We thank Shun Zhao, Jun Liao, Hua Li, and Dong Wu for support on solving the structure. We thank Ke-qiong Ye, Jia-wei Wu, Xue-wu Zhang for insightful suggestions and comments. We thank the Shanghai Synchrotron Radiation Facility (SSRF) BL18U for help with X-ray data collection. This work was supported by grants from the National Natural Science Foundation of China (31670846, 31721002, and 31670850), the National Key Basic Research Program of China (2015CB910800), and funds from Huazhong University of Science and Technology.

Author contributions

XW, XiaoyY, and JG generated all mutants. XW performed and analyzed biochemical and structural experiments. JG performed electrophysiology and imaging experiments. SW and XW performed single-molecule FRET experiments. LZ and YX performed Munc18-1/Habc/H3 assembly experiments. XW, JG, SW, and CM wrote the manuscript. CM and XiaofY conceived the experiments. CM supervised the study.

Conflict of interest

The authors declare that they have no conflict of interest.

References

- Arunachalam L, Han L, Tassew NG, He Y, Wang L, Xie L, Fujita Y, Kwan E, Davletov B, Monnier PP *et al* (2008) Munc18-1 is critical for plasma membrane localization of syntaxin1 but not of SNAP-25 in PC12 cells. *Mol Biol Cell* 19: 722–734
- Augustin I, Rosenmund C, Südhof TC, Brose N (1999) Munc13-1 is essential for fusion competence of glutamatergic synaptic vesicles. *Nature* 400: 457–461
- Baker RW, Jeffrey PD, Hughson FM (2013) Crystal structures of the Sec1/Munc18 (SM) protein Vps33, alone and bound to the homotypic fusion and vacuolar protein sorting (HOPS) subunit Vps16*. *PLoS ONE* 8: e67409
- Baker RW, Jeffrey PD, Zick M, Phillips BP, Wickner WT, Hughson FM (2015) A direct role for the Sec1/Munc18-family protein Vps33 as a template for SNARE assembly. *Science* 349: 1111–1114
- Baker RW, Hughson FM (2016) Chaperoning SNARE assembly and disassembly. *Nat Rev Mol Cell Biol* 17: 465–479
- Bar-On D, Nachliel E, Gutman M, Ashery U (2011) Dynamic conformational changes in munc18 prevent syntaxin binding. *PLoS Comput Biol* 7: e1001097
- Brunger AT (2005) Structure and function of SNARE and SNARE-interacting proteins. *Q Rev Biophys* 38: 1–47
- Brunger AT, Choi UB, Lai Y, Leitz J, White KI, Zhou Q (2019) The pre-synaptic fusion machinery. *Curr Opin Struct Biol* 54: 179–188
- Burkhardt P, Hattendorf DA, Weis WI, Fasshauer D (2008) Munc18a controls SNARE assembly through its interaction with the syntaxin N-peptide. *EMBO J* 27: 923–933
- Colbert KN, Hattendorf DA, Weiss TM, Burkhardt P, Fasshauer D, Weis WI (2013) Syntaxin1a variants lacking an N-peptide or bearing the LE mutation bind to Munc18a in a closed conformation. *Proc Natl Acad Sci USA* 110: 12637–12642
- Collins BM, Martin JL (2015) SEC-uring membrane fusion: a sneak peek at SNARE-complex assembly driven by Sec1-Munc18 proteins. *Nat Struct Mol Biol* 22: 756–758
- Diao J, Ishitsuka Y, Lee H, Joo C, Su Z, Syed S, Shin YK, Yoon TY, Ha T (2012) A single vesicle-vesicle fusion assay for *in vitro* studies of SNAREs and accessory proteins. *Nat Protoc* 7: 921–934
- Dulubova I, Sugita S, Hill S, Hosaka M, Fernandez I, Südhof TC, Rizo J (1999) A conformational switch in syntaxin during exocytosis: role of munc18. *EMBO J* 18: 4372–4382
- Dulubova I, Khvotchev M, Liu S, Huryeva I, Südhof TC, Rizo J (2007) Munc18-1 binds directly to the neuronal SNARE complex. *Proc Natl Acad Sci USA* 104: 2697–2702
- Emsley P, Lohkamp B, Scott WG, Cowtan K (2010) Features and development of Coot. *Acta Crystallogr D Biol Crystallogr* 66: 486–501
- Gerber SH, Rah JC, Min SW, Liu X, de Wit H, Dulubova I, Meyer AC, Rizo J, Arancillo M, Hammer RE *et al* (2008) Conformational switch of syntaxin-1 controls synaptic vesicle fusion. *Science* 321: 1507–1510
- Hammarlund M, Palfreyman MT, Watanabe S, Olsen S, Jorgensen EM (2007) Open syntaxin docks synaptic vesicles. *PLoS Biol* 5: e198
- Han L, Jiang T, Han GA, Malintan NT, Xie L, Wang L, Tse FW, Gaisano HY, Collins BM, Meunier FA *et al* (2009) Rescue of Munc18-1 and -2 double knockdown reveals the essential functions of interaction between Munc18 and closed syntaxin in PC12 cells. *Mol Biol Cell* 20: 4962–4975
- Han GA, Malintan NT, Saw NM, Li L, Han L, Meunier FA, Collins BM, Sugita S (2011) Munc18-1 domain-1 controls vesicle docking and secretion by

- interacting with syntaxin-1 and chaperoning it to the plasma membrane. *Mol Biol Cell* 22: 4134–4149
- Han GA, Bin NR, Kang SY, Han L, Sugita S (2013) Domain 3a of Munc18-1 plays a crucial role at the priming stage of exocytosis. *J Cell Sci* 126: 2361–2371
- Han GA, Park S, Bin NR, Jung CH, Kim B, Chandrasegaram P, Matsuda M, Riadi I, Han L, Sugita S (2014) A pivotal role for pro-335 in balancing the dual functions of Munc18-1 domain-3a in regulated exocytosis. *J Biol Chem* 289: 33617–33628
- He E, Wierda K, van Westen R, Broeke JH, Toonen RF, Cornelisse LN, Verhage M (2017) Munc13-1 and Munc18-1 together prevent NSF-dependent de-priming of synaptic vesicles. *Nat Commun* 8: 15915
- Hu SH, Christie MP, Saez NJ, Latham CF, Jarrott R, Lua LH, Collins BM, Martin JL (2011) Possible roles for Munc18-1 domain 3a and Syntaxin1 N-peptide and C-terminal anchor in SNARE complex formation. *Proc Natl Acad Sci USA* 108: 1040–1045
- Imig C, Min S-W, Krinner S, Arancillo M, Rosenmund C, Südhof TC, Rhee J, Brose N, Cooper BH (2014) The morphological and molecular nature of synaptic vesicle priming at presynaptic active zones. *Neuron* 84: 416–431
- Jahn R, Scheller RH (2006) SNAREs—engines for membrane fusion. *Nat Rev Mol Cell Biol* 7: 631–643
- Jahn R, Fasshauer D (2012) Molecular machines governing exocytosis of synaptic vesicles. *Nature* 490: 201–207
- James DJ, Martin TF (2013) CAPS and Munc13: CATCHRs that SNARE vesicles. *Front Endocrinol* 4: 187
- Jiao J, He M, Port SA, Baker RW, Xu Y, Qu H, Xiong Y, Wang Y, Jin H, Eisemann TJ et al (2018) Munc18-1 catalyzes neuronal SNARE assembly by templating SNARE association. *Elife* 7: e41771
- Joo C, Ha T (2012) Single-molecule FRET with total internal reflection microscopy. *Cold Spring Harb Protoc* 2012: pdb.top072058
- Kreutzberger AJB, Kiessling V, Stroupe C, Liang B, Preobraschenski J, Ganzella M, Kreutzberger MAB, Nakamoto R, Jahn R, Castle JD et al (2019) *In vitro* fusion of single synaptic and dense core vesicles reproduces key physiological properties. *Nat Commun* 10: 3904
- Lai Y, Choi UB, Leitz J, Rhee HJ, Lee C, Altas B, Zhao M, Pfuetzner RA, Wang AL, Brose N et al (2017) Molecular mechanisms of synaptic vesicle priming by Munc13 and Munc18. *Neuron* 95: 591–607 e510
- Laufman O, Kedan A, Hong W, Lev S (2009) Direct interaction between the COG complex and the SM protein, Sly1, is required for Golgi SNARE pairing. *EMBO J* 28: 2006–2017
- Ma C, Li W, Xu Y, Rizo J (2011) Munc13 mediates the transition from the closed syntaxin-Munc18 complex to the SNARE complex. *Nat Struct Mol Biol* 18: 542–549
- Ma C, Su L, Seven AB, Xu Y, Rizo J (2013) Reconstitution of the vital functions of Munc18 and Munc13 in neurotransmitter release. *Science* 339: 421–425
- Ma L, Rebane AA, Yang G, Xi Z, Kang Y, Gao Y, Zhang Y (2015) Munc18-1-regulated stage-wise SNARE assembly underlying synaptic exocytosis. *Elife* 4: e09580
- Malsam J, Kreye S, Söllner TH (2008) Membrane fusion: SNAREs and regulation. *Cell Mol Life Sci* 65: 2814–2832
- Margittai M, Fasshauer D, Jahn R, Langen R (2003) The Habc domain and the SNARE core complex are connected by a highly flexible linker. *Biochemistry* 42: 4009–4014
- Martin S, Tomatis VM, Papadopoulos A, Christie MP, Malintan NT, Gormal RS, Sugita S, Martin JL, Collins BM, Meunier FA (2013) The Munc18-1 domain 3a loop is essential for neuroexocytosis but not for syntaxin-1A transport to the plasma membrane. *J Cell Sci* 126: 2353–2360
- McCoy AJ, Grosse-Kunstleve RW, Adams PD, Winn MD, Storoni LC, Read RJ (2007) Phaser crystallographic software. *J Appl Crystallogr* 40: 658–674
- Misura KM, Scheller RH, Weis WI (2000) Three-dimensional structure of the neuronal-Sec1-syntaxin 1a complex. *Nature* 404: 355–362
- Misura KM, Scheller RH, Weis WI (2001) Self-association of the H3 region of syntaxin 1a implications for intermediates in snare complex assembly. *J Biol Chem* 276: 13273–13282
- Morgera F, Sallah MR, Dubuke ML, Gandhi P, Brewer DN, Carr CM, Munson M (2012) Regulation of exocytosis by the exocyst subunit Sec6 and the SM protein Sec1. *Mol Biol Cell* 23: 337–346
- Munch AS, Kedar GH, van Weering JR, Vazquez-Sanchez S, He E, André T, Braun T, Söllner TH, Verhage M, Sørensen JB (2016) Extension of helix 12 in Munc18-1 induces vesicle priming. *J Neurosci* 36: 6881–6891
- Parisotto D, Pfau M, Scheutzow A, Wild K, Mayer MP, Malsam J, Sinning I, Söllner TH (2014) An extended helical conformation in domain 3a of Munc18-1 provides a template for SNARE (soluble N-ethylmaleimide-sensitive factor attachment protein receptor) complex assembly. *J Biol Chem* 289: 9639–9650
- Park S, Bin NR, Yu B, Wong R, Sitarska E, Sugita K, Ma K, Xu J, Tien CW, Algouneh A et al (2017) UNC-18 and tomosyn antagonistically control synaptic vesicle priming downstream of UNC-13 in *Caenorhabditis elegans*. *J Neurosci* 37: 8797–8815
- Richmond JE, Weimer RM, Jorgensen EM (2001) An open form of syntaxin bypasses the requirement for UNC-13 in vesicle priming. *Nature* 412: 338–341
- Rizo J, Südhof TC (2012) The membrane fusion enigma: SNAREs, Sec1/Munc18 proteins, and their accomplices—guilty as charged? *Annu Rev Cell Dev Biol* 28: 279–308
- Rizo J, Xu J (2015) The synaptic vesicle release machinery. *Annu Rev Biophys* 44: 339–367
- Rodkey TL, Liu S, Barry M, McNew JA (2008) Munc18a scaffolds SNARE assembly to promote membrane fusion. *Mol Biol Cell* 19: 5422–5434
- Rosenmund C, Stevens CF (1996) Definition of the readily releasable pool of vesicles at hippocampal synapses. *Neuron* 16: 1197–1207
- Servant G, Weiner OD, Neptune ER, Sedat JW, Bourne HR (1999) Dynamics of a chemoattractant receptor in living neutrophils during chemotaxis. *Mol Biol Cell* 10: 1163–1178
- Shen J, Tareste DC, Paumet F, Rothman JE, Melia TJ (2007) Selective activation of cognate SNAREpins by Sec1/Munc18 proteins. *Cell* 128: 183–195
- Shu T, Jin H, Rothman JE, Zhang Y (2020) Munc13-1 MUN domain and Munc18-1 cooperatively chaperone SNARE assembly through a tetrameric complex. *Proc Natl Acad Sci USA* 117: 1036–1041
- Sitarska E, Xu J, Park S, Liu X, Quade B, Stepien K, Sugita K, Brautigam CA, Sugita S, Rizo J (2017) Autoinhibition of Munc18-1 modulates synaptobrevin binding and helps to enable Munc13-dependent regulation of membrane fusion. *Elife* 6: e24278
- Stein A, Weber G, Wahl MC, Jahn R (2009) Helical extension of the neuronal SNARE complex into the membrane. *Nature* 460: 525–528
- Stepien KP, Prinslow EA, Rizo J (2019) Munc18-1 is crucial to overcome the inhibition of synaptic vesicle fusion by α SNAP. *Nat Commun* 10: 1–18
- Südhof TC, Rothman JE (2009) Membrane fusion: grappling with SNARE and SM proteins. *Science* 323: 474–477
- Südhof TC, Rizo J (2011) Synaptic vesicle exocytosis. *Cold Spring Harb Perspect Biol* 3: a005637
- Sutton RB, Fasshauer D, Jahn R, Brunger AT (1998) Crystal structure of a SNARE complex involved in synaptic exocytosis at 2.4 Å resolution. *Nature* 395: 347–353

- Taresté D, Shen J, Melia TJ, Rothman JE (2008) SNAREpin/Munc18 promotes adhesion and fusion of large vesicles to giant membranes. *Proc Natl Acad Sci USA* 105: 2380–2385
- Toonen RF, Kochubey O, de Wit H, Gulyas-Kovacs A, Konijnenburg B, Sørensen JB, Klingauf J, Verhage M (2006) Dissecting docking and tethering of secretory vesicles at the target membrane. *EMBO J* 25: 3725–3737
- Varoqueaux F, Sigler A, Rhee JS, Brose N, Enk C, Reim K, Rosenmund C (2002) Total arrest of spontaneous and evoked synaptic transmission but normal synaptogenesis in the absence of Munc13-mediated vesicle priming. *Proc Natl Acad Sci USA* 99: 9037–9042
- Voets T, Toonen RF, Brian EC, de Wit H, Moser T, Rettig J, Südhof TC, Neher E, Verhage M (2001) Munc18-1 promotes large dense-core vesicle docking. *Neuron* 31: 581–591
- Wang S, Choi UB, Gong J, Yang X, Li Y, Wang AL, Yang X, Brunger AT, Ma C (2017) Conformational change of syntaxin linker region induced by Munc13s initiates SNARE complex formation in synaptic exocytosis. *EMBO J* 36: 816–829
- Wang S, Li Y, Gong J, Ye S, Yang X, Zhang R, Ma C (2019) Munc18 and Munc13 serve as a functional template to orchestrate neuronal SNARE complex assembly. *Nat Commun* 10: 69
- Weber T, Zemelman BV, McNew JA, Westermann B, Gmachl M, Parlati F, Söllner TH, Rothman JE (1998) SNAREpins: minimal machinery for membrane fusion. *Cell* 92: 759–772
- Wickner W (2010) Membrane fusion: five lipids, four SNAREs, three chaperones, two nucleotides, and a Rab, all dancing in a ring on yeast vacuoles. *Annu Rev Cell Dev Biol* 26: 115–136
- Yang B, Steegmaier M, Gonzalez LC Jr, Scheller RH (2000) nSec1 binds a closed conformation of syntaxin1A. *J Cell Biol* 148: 247–252
- Yang X, Wang S, Sheng Y, Zhang M, Zou W, Wu L, Kang L, Rizo J, Zhang R, Xu T et al (2015) Syntaxin opening by the MUN domain underlies the function of Munc13 in synaptic-vesicle priming. *Nat Struct Mol Biol* 22: 547–554
- Yu H, Shen C, Liu Y, Menasche BL, Ouyang Y, Stowell MHB, Shen J (2018) SNARE zippering requires activation by SNARE-like peptides in Sec1/Munc18 proteins. *Proc Natl Acad Sci USA* 115: E8421–E8429